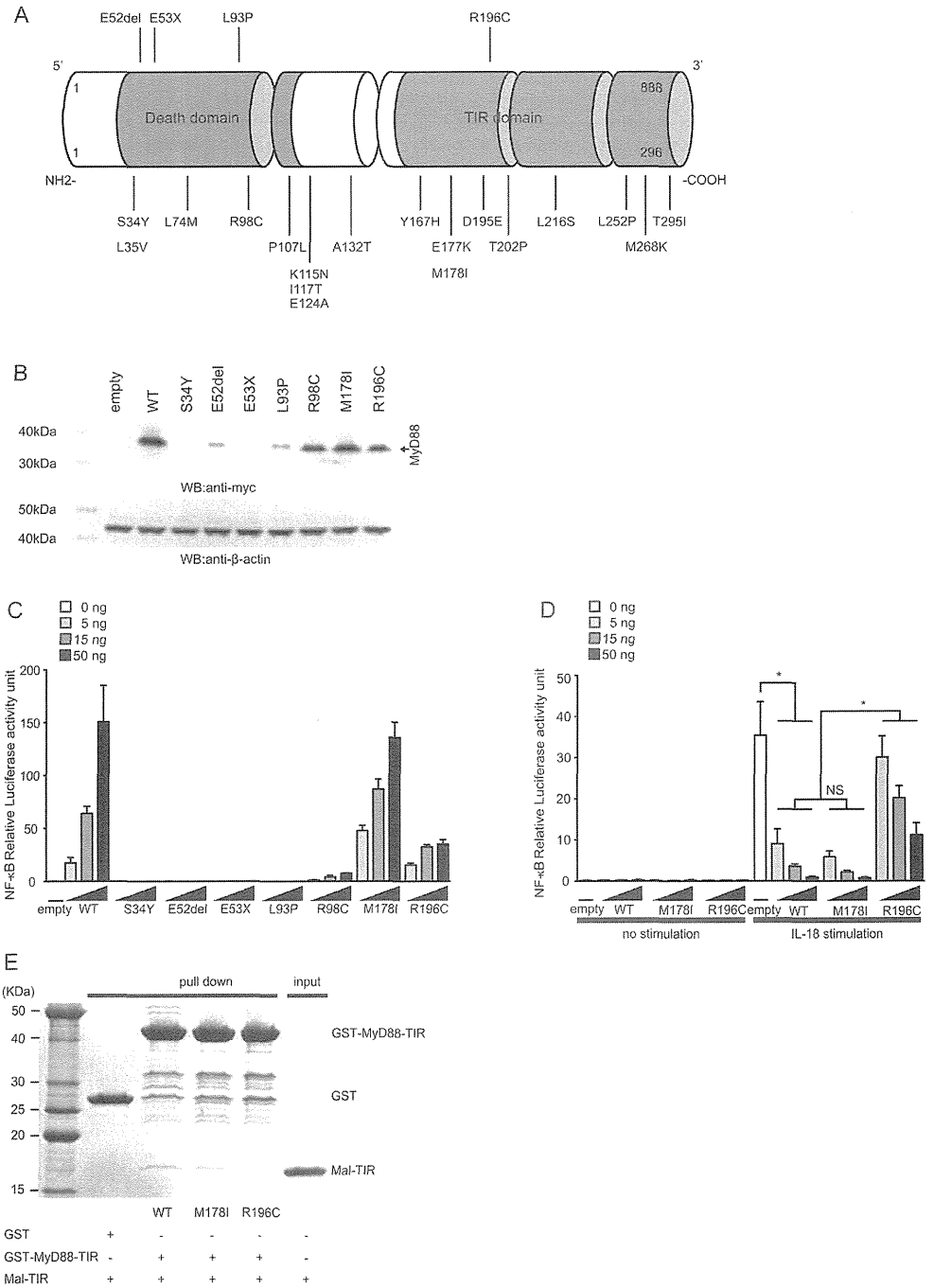

Fig. 3. Cell-based assays of *MyD88* variants. (A) Schematic representation of *MyD88* with all identified mutations and nonsynonymous SNPs. *MyD88* consists of five exons and the protein is composed of an N terminal death domain and C-terminal TIR domain. Mutations are annotated at the upper side of this schema, and SNPs at the lower. (B) Expression levels of *MyD88* variants in HEK293T cells. The protein expression of S34Y and E53X could not be detected, and that of E52del and L93P was very low. The expression levels of R98C, M178I, and R196C were similar to that of WT. (C) NF-κB reporter gene activities of *MyD88* variants in HEK293T cells. S34Y, E52del, E53X, L93P, R98C, and R196C were compromised in the ability to enhance NF-κB activation, with the exception of M178I. (D) Dominant negative inhibitory effects of MyD88-TIR variants in HEK293T cells. MyD88-TIR R196C failed to inhibit NF-κB activation. Data represent the mean ± SD of a representative experiment ($n = 3$). All data were compared at each transfection dose. Asterisk indicates statistically significant difference between WT and the others. NS means "not-significant". (E) Binding assays for WT or mutant MyD88-TIRs with Mal-TIR using GST pull-down assays. M178I interacted with Mal-TIR as well as WT. R196C showed a reduced interaction with Mal-TIR.

located in the TIR domain of MyD88, we carried out a GST pull-down assay of MyD88-TIR and Mal-TIR (Fig. 3E). As we reported previously (Nada et al., 2012; Ohnishi et al., 2009), MyD88-TIR R196C showed a significant decrease in its ability to directly bind to Mal-TIR, while MyD88-TIR M178I interacted with Mal-TIR as well as WT.

3.4. Analytical gel filtration of IRAK4 and MyD88

To compare the interaction between MyD88 and IRAK4, analytical gel filtration was carried out. We purified MyD88-DD + IDs and IRAK4-DD + IDs recombinant proteins, and analyzed the elution profiles of mixtures of MyD88 WT or mutants in the presence

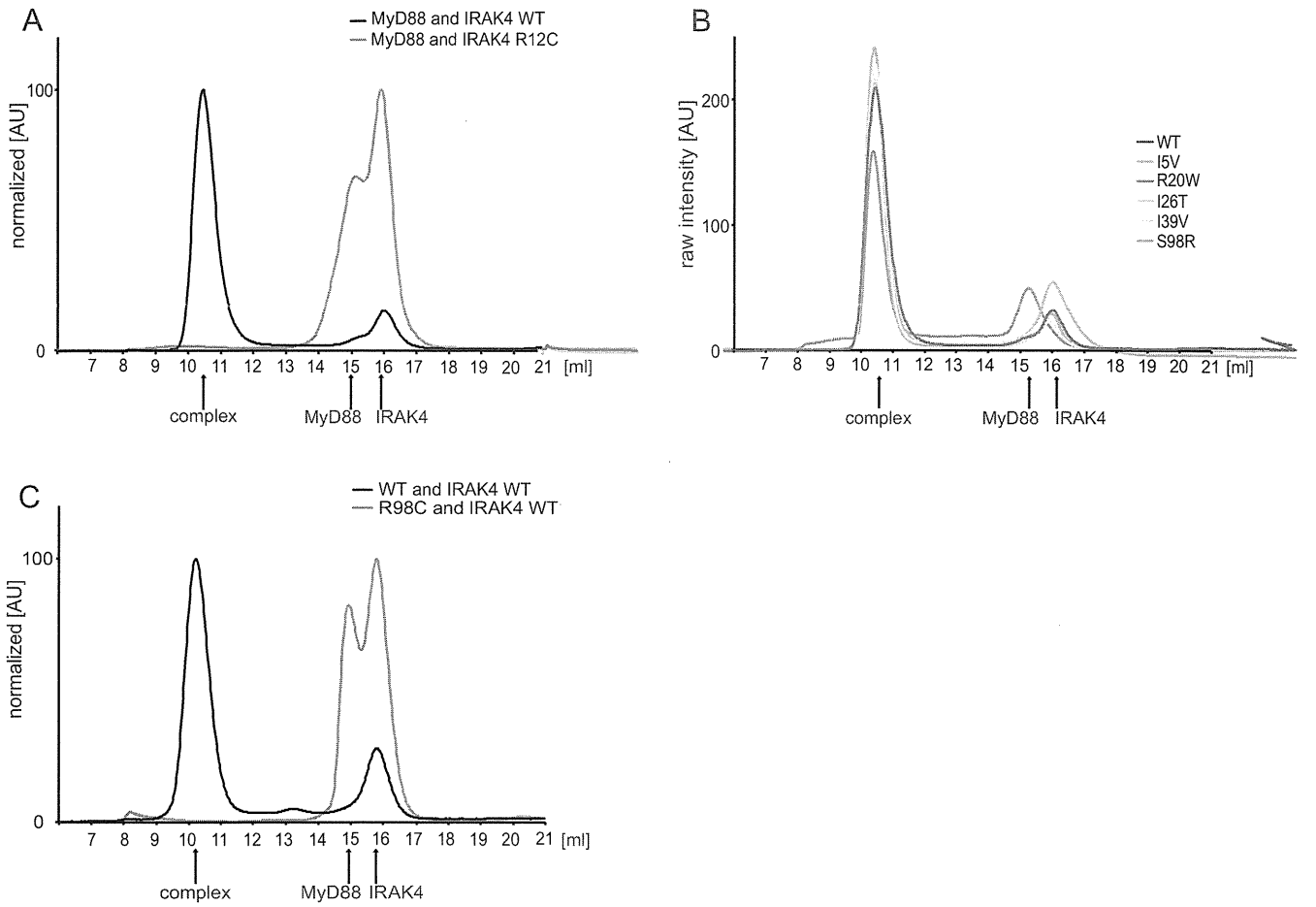

Fig. 4. Analytical gel filtration of IRAK4 and MyD88. (A) IRAK4-R12C failed to interact with MyD88. R12C was unable to assemble into a Myddosome as shown by size exclusion chromatography of mixtures of bacterially purified MyD88-DD + IDs and IRAK4-DD + IDs (added in excess). MyD88-DD + ID WT + IRAK4-DD + ID WT mixture eluted in a discrete complex peak that was absent from R12C mixtures. (B) IRAK4 SNPs interacted with MyD88 WT. Only IRAK4 R20W showed a decreased peak intensity of complete complex and residual peak of MyD88-DD + ID despite mixing an excess of IRAK4. (C) MyD88-R98C failed to interact with IRAK4. Individual peak fractions from gel filtration, purified MyD88-DD + ID or IRAK4-DD + ID alone (for size comparison) were analyzed by reducing SDS-PAGE (data not shown).

of a molar excess of IRAK4-DD + ID WT or mutants. Individual fractions or purified reference proteins were analyzed by SDS-PAGE (data not shown). The estimated molecular weights were calculated using a calibration curve, and were 30.6 kDa, 48.3 kDa, and 423 kDa for IRAK4-DD + ID, MyD88-DD + ID, and their complex, respectively. Although IRAK4-DD was eluted as a 1mer (George et al., 2011; Lin et al., 2010; Motshwene et al., 2009), IRAK4-DD + ID was mainly eluted as a 2mer. While MyD88 was mainly eluted as a 3mer. IRAK4 WT formed a characteristic oligomer by mixing with MyD88 WT, but not R98C, as previously reported (Fig. 4C) (Nagpal et al., 2011). Moreover, IRAK4 R12C also failed to form a complex (Fig. 4A). By contrast, *IRAK4* SNPs interacted with MyD88 WT (Fig. 4B), but only IRAK4 R20W showed a decreased intensity of the complex and residual peak of MyD88-DD + ID, despite an excess amount of IRAK4.

3.5. NMR titration

The IRAK4–MyD88 interaction was also examined using NMR spectroscopy for which 2D ^{1}H–^{15}N correlation NMR spectra of ^{15}N-labeled MyD88-DD + ID were recorded in the presence or absence of various concentrations of IRAK4-DD + ID or its derivatives. Changes of NMR signal intensities of a Trp residue in ^{15}N-labeled MyD88-DD + ID following titration were used to monitor the interaction (Fig. 5). The normalized NMR signal intensity steeply decreased upon IRAK4 titration. Attenuation of the NMR signal could be

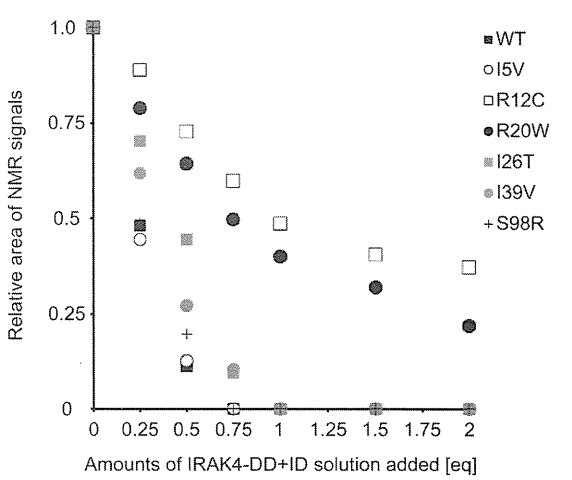

Fig. 5. NMR titration study of ^{1}H–^{15}N-MyD88-DD + ID and IRAK4-DD + ID. Normalized intensities of NMR signals, obtained from the NMR titration experiment (Supplemental Fig. S1), were plotted in a function of equivalent moles (eq) of IRAK4-DD + ID added to ^{15}N-MyD88-DD + ID. The attenuation of signal intensities was presumably caused by formation of complexes between MyD88-DD + ID and IRAK4-DD + ID. NMR signal attenuation of R12C and R20W was significantly suppressed relative to WT, indicating a weak affinity for MyD88-DD + ID. Black box, white circle, white box, black circle, gray box, gray circle, and black cross indicate the normalized intensities of WT, I5V, R12C, R20W, I26T, I39V, and S98R, respectively.

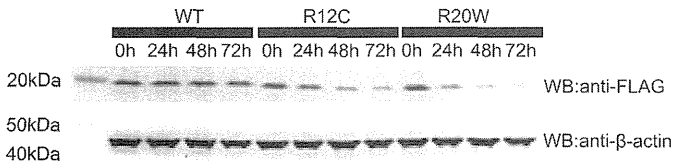

Fig. 6. Stability of IRAK4-DD variants in HEK293T cells. Cells were incubated in cycloheximide (25 μM) for the indicated times before preparation of cell extracts for SDS-PAGE separation and immunoblotting with an anti-FLAG antibody. IRAK4-DD WT maintained a steady state of protein structure, but R20W began to collapse after 24 h.

interpreted as a result of the formation of large protein complexes involving ^{15}N-labeled MyD88-DD + ID, indicating an interaction of the titrated IRAK4-DD + ID with ^{15}N-MyD88-DD + ID. Four IRAK4 derivatives, I5V, I26T, I39V, and S98R, showed a similar attenuation pattern to that of WT. By contrast, attenuation of NMR signal intensities was significantly suppressed when one of two derivatives, R12C or R20W, was used as a titrant. These observations suggest that the affinity of R12C and R20W towards MyD88-DD + ID was weaker than that of WT.

3.6. Instability of IRAK4 R12C and R20W

In the analytical gel filtration and NMR titration assays, IRAK4 R12C failed to interact with MyD88. On the other hand, IRAK4 R20W could interact with MyD88, but the amount of complete complex was lower than WT and other SNPs. Additionally, R12C and R20W were predicted to be "probably damaging" with scores of 1.000 and 0.998, respectively, by the PolyPhen-2 algorithm (http://genetics.bwh.harvard.edu/pph2/) (Adzhubei et al., 2010). Therefore, we next evaluated the protein stability of IRAK4-DD + ID R12C and R20W compared with WT following treatment with cycloheximide (Fig. 6). IRAK4-DD + ID WT protein levels did not change during 72 h of cycloheximide treatment, but R12C protein levels slightly decreased after 48 h of treatment, and R20W protein levels decreased after 24 h of treatment.

4. Discussion

4.1. In vitro assays for assessments of the mutational effects of human IRAK4 gene

Several cell-based functional assays of *IRAK4* mutants have previously been described, but the mutational effects of novel mutations have not been confirmed. For example, Lye et al. examined the NF-κB activation of *IRAK4* mutants using IRAK4-knocked out murine fibroblasts (Lye et al., 2004), while Qin et al. (2004) used human fibroblasts derived from an IRAK4 deficiency patient. Medvedev et al. (2005) examined the IL-1 signaling complex formation of an *IRAK4* mutant using immunoprecipitation. In the present study, we examined selected *IRAK4* mutations, including three previously reported missense mutations (Fig. 1A). Protein expression levels of WT and R12C were similar (Fig. 1B), so we then assessed the signaling function using HEK293T cells (Medvedev et al., 2003) as it is difficult to obtain an IRAK4-deficient human cell line. IRAK4 Q293X protein expression was undetectable and it did not appear to inhibit NF-κB activity (Figs. 1B and 2G), which agrees with the results of Medvedev et al. (2003).

The other *IRAK4* mutants, with the exception of R12C which expressed undetectable or low level IRAK4 protein, also did not inhibit NF-κB activity. On the other hand, R12C inhibited NF-κB activity to almost the same extent as WT. This suggests that overexpressed IRAK4 protein only inhibits NF-κB activity when full-length IRAK4 is expressed at levels above a certain threshold. All SNPs analyzed expressed similar protein levels and inhibited NF-κB activity to the same level as WT (Fig. 1C and E). Interestingly, R20W showed a significantly stronger inhibition of NF-κB activity than WT and other SNPs, while the PolyPhen-2 algorithm "probably damaging" prediction for R12C and R20W meant that the behavior of both was uncertain.

To clarify this, we focused on these two variants. From information about the Myddosome protein structure (PDB code: 3MOP) (Lin et al., 2010), residues R12 and R20 appeared to be located on the surface of IRAK4-DD, in the interface between IRAK4 and MyD88, and to directly interact with MyD88-DD E102 and D46, respectively (Fig. 7B). A protein–protein interaction study was used to assess the mutational effect of these residues. MyD88-DD R98 was located in the interface to IRAK4-DD (George et al., 2011), while MyD88-TIR R196 was located in the interface to Mal-TIR (Ohnishi et al., 2009). These arginine to cysteine substitutions caused a change in protein–protein interaction abilities. The recombinant proteins of IRAK4-DD + ID WT and MyD88-DD + ID WT formed a higher order oligomeric complex, but IRAK4 R12C failed to interact with MyD88.

While we were preparing this manuscript, T77del, a novel mutation of human IRAK4 deficiency, was reported as a loss-of-expression variant following a western blot of a patient's fibroblasts (Andres et al., 2013). Lin et al. (2010) used immunoprecipitation to show that both T76 and N78 are critical residues for the interaction with MyD88. Therefore T77 might be critical not only for protein expression but also the interaction with MyD88. It should be noted that although IRAK4 S98 is located on the surface of IRAK4-DD (Fig. 7A), it is distant from the interface with MyD88-DD. From the complex structural information, S98 might be located in the interface between IRAK4 and IRAK2. Future work should carry out a protein interaction study between IRAK4 S98R and IRAK2 or IRAK1 to evaluate the pathogenicity of IRAK4 S98R.

All *IRAK4* SNPs examined in the present study formed a complex in analytical gel filtration. Interestingly, R20W also formed a complex, albeit less than WT and the other SNPs. In addition, an incomplete complex of IRAK4 R20W and MyD88 was observed between the peak of unbound proteins and complete complex (Fig. 4B). Moreover, the NMR signal attenuation titrated with IRAK4 R12C and R20W was reduced compared with WT (Fig. 5), suggesting that the interaction was weakened by amino acid substitutions. From these results, we speculated that not only the mild loss of protein–protein interaction, but also the loss of IRAK4-DD R20W protein stability inhibits the formation of a complete complex of IRAK4 and MyD88. Therefore, we examined protein stability using cycloheximide. The stability of IRAK4-DD R12C was slightly lower, but that of R20W was much lower than WT and R12C (Fig. 6). Thus it is conceivable that the hydrophilic Arg20 substitution to hydrophobic tryptophan reduces the stability of the protein structure. Finally, we propose the possibility that not only IRAK4 R12C but also R20W has an impact on human IRAK4 deficiency (Table 1).

4.2. In vitro assays for assessments of the mutational effects of human MyD88 gene

Recently, the loss-of-function variants S34Y and R98C were found in naturally occurring *MyD88* SNPs (George et al., 2011; Nagpal et al., 2011). The functions of these variants were also shown by a luciferase reporter gene assay in HEK293 I3A cells, and interaction analysis with recombinant proteins. On the other hand, Napgal et al. carried out an initial functional assay of *MyD88* variants using a luciferase reporter gene assay in HEK293T cells, which are not MyD88-deficient. In addition, Loiarro et al. (2009) used immunoprecipitation in HEK293T cells to indicate that E52 and Y58 were key residues that interact with both IRAK1 and IRAK4, and that K95 was an important residue to interact with IRAK4. In this

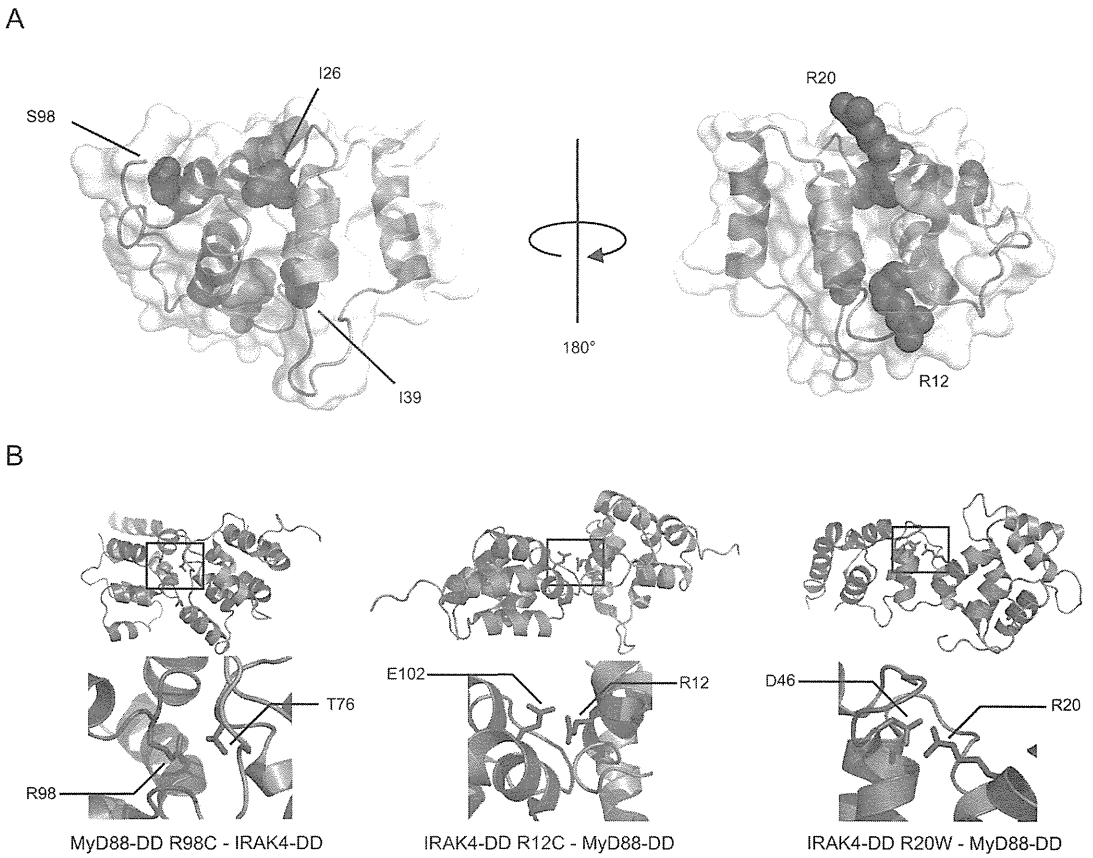

Fig. 7. Protein structure of IRAK4-DD. (A) Schematic representation of IRAK4-DD (Protein Data Bank accession code 2A9I) generated with PyMOL (DeLano Scientific, www.pymol.org). Mutants and variants are shown as red full-surface amino acid residues. R12, R20, and S98 are located on the surface of IRAK4-DD. (B) 3D interaction models of IRAK4-DD (green) with MyD88-DD (orange). MyD88-DD R98 (side chain shown as a blue stick) interacts with IRAK4-DD T76. IRAK4-DD R12 and R20 (side chains shown as red sticks) interact with MyD88-DD E102 and D46, respectively.

study, we revealed decreased protein expression levels of *MyD88* variants (S34Y, E52del, and L93P) with HEK293T cells, indicating that they have unstable protein structures (Fig. 3B). Moreover, R98C as well as the loss-of-expression variants had lower NF-κB activity than MyD88 WT (Fig. 3C), while MyD88-DD R98C had an impaired direct interaction with IRAK4-DD WT (Fig. 4C). Consequently, MyD88 R98C can be a risk-allele for MyD88 deficiency, because it showed similar to IRAK4 R12C about the results of interaction assay between MyD88-DD and IRAK4-DD. Thus, the results of MyD88-DD gene variation from a cell-based assay using a MyD88-non-deficient cell line are consistent with the protein interaction study, unlike the *IRAK4* variants.

MyD88 interacts with Mal via a shared TIR domain. We previously found that MyD88-TIR R196C had stable protein folding but a significant decrease in its ability to directly bind Mal-TIR (Nada et al., 2012; Ohnishi et al., 2009). TIR domains have an important functional region, the BB loop, which interacts with other TIR domain-containing proteins. As the R196C mutation and M178I SNP are located in or near the BB loop of the MyD88 TIR domain, we tested MyD88 full-length-induced NF-κB activation and the inhibition of ligand-induced NF-κB activity caused by a dominant-negative effect to assess the functional effect of M178I. MyD88 full-length M178I significantly enhanced NF-κB activity, as seen in WT (Fig. 3C). MyD88-TIR M178I inhibited NF-κB activation to the same extent as WT, but R196C did not (Fig. 3D). Furthermore, a GST pull-down assay using recombinant purified proteins found that MyD88-TIR M178I interacted with Mal-TIR as well as WT (Fig. 3E), which was consistent with the cell-based assays. Therefore we determined M178I to be a variant, although the mutation of a neighboring residue, I179N also called the Poc

Table 1
Summary of the expression and functional analysis of *IRAK4* variants.

Gene	Variant	Protein expression	NF-κB activity	Interaction	Protein stability	Pathogenicity
IRAK4	M1V	Absent	–	–	–	Reported
	I5V	Normal	Inhibited	Normal	–	Polymorphism
	R12C	Normal	Inhibited	Reduced	Mild reduced	Reported
	R20W	Normal	Inhibited	Mild reduced	Reduced	Probable
	I26T	Normal	Inhibited	Normal	–	Polymorphism
	I39V	Normal	Inhibited	Normal	–	Polymorphism
	c.118insA	Severely reduced	Not inhibited	–	–	Reported
	S98R	Normal	Inhibited	Normal	–	Polymorphism
	R183X	Truncated	Not inhibited	–	–	Reported
	Q293X	Severely reduced	Not inhibited	–	–	Reported
	G298D	Reduced	Not inhibited	–	–	Reported

Table 2
Summary of the expression and functional analysis of *MyD88* variants.

Gene	Variant	Protein expression	NF-κB activity	Interaction	Pathogenicity
MyD88	S34Y	Severely reduced	Not enhanced	–	Probable
	E52del	Reduced	Not enhanced	–	Reported
	E53X	Severely reduced	Not enhanced	–	Reported
	L93P	Reduced	Not enhanced	–	Reported
	R98C	Normal	Not enhanced	Reduced	Probable
	M178I	Normal	Enhanced	Normal	Polymorphism
	R196C	Normal	Not enhanced	Reduced	Reported

mutation, is associated with a loss-of-function of MyD88 (Jiang et al., 2006).

In Table 2, we summarize the functional phenotypes of *MyD88* mutations and SNPs described in this study. Our results suggest that the mutational effects of *MyD88* variants, at least those located in DD and TIR domains, can only be assessed by cell-based reporter gene assays using widely available cell lines such as HEK293 cells, unlike *IRAK4* variants.

4.3. The additional discussion about another components of Myddosome, Mal

Recently, several functional assays of variants of Mal, located in the TIR domain have been reported. Nagpal et al. (2009) found that Mal D96N was unable to interact with MyD88 using a reporter gene assay and immunoprecipitation, while George et al. (2010) confirmed this by immunofluorescence. We used a reporter gene assay to show that E132K, R143Q, and E190D are loss of functional variants (An et al., 2011). E132K is of particular importance as it is located in the BB loop of the Mal TIR domain, so we speculate that it might be a pathogenic mutation of Mal deficiency. More recently, Weller et al. (2012) reported that Mal R121W, which is also located in the Mal BB loop at a similar site to R196C of *MyD88*, causes human Mal deficiency. Therefore, future work should examine the functions of the gene variants of not only IRAK4 and MyD88 but also Mal deposited in the SNP database.

5. Conclusion

Not only previously reported loss-of-function mutations but also several SNPs are considered likely to be pathogenic for human diseases, because of their loss of functions proved by *in vitro* methods. Loss of protein stability and defect of interaction between the components of Myddosome may cause IRAK4 and MyD88 deficiencies as a result of a failure to form a precise Myddosome structure. Our findings indicate that the analysis of Myddosome formation with recombinant proteins is useful to distinguish whether missense mutations, especially those located in the DD of IRAK4, are causative. Thus, the combination of *in vitro* functional assays is effective to confirm pathogenicity of mutants found in IRAK4 and MyD88 deficiency patients.

Acknowledgments

We thank Kasahara, K., Yamamoto, M., Tsuji, K. and Sakaguchi, N. for technical assistance. We thank the members of the research group of human *IRAK4* deficiency in Japan for their collaboration. This work was supported by Grants-in-Aid for Scientific Research from the Ministry of Education, Culture, Sports, Science and Technology of Japan and by Health and Labour Science Research Grants for Research on Intractable Diseases from the Ministry of Health, Labour and Welfare.

Appendix A. Supplementary data

Supplementary data associated with this article can be found, in the online version, at http://dx.doi.org/10.1016/j.molimm.2013.11.008.

References

Adzhubei, I.A., Schmidt, S., Peshkin, L., Ramensky, V.E., Gerasimova, A., Bork, P., Kondrashov, A.S., Sunyaev, S.R., 2010. A method and server for predicting damaging missense mutations. Nature Methods 7, 248–249.

Al-Herz, W., Bousfiha, A., Casanova, J.-L., Chapel, H., Conley, M.E., Cunningham-Rundles, C., Etzioni, A., Fischer, A., Franco, J.L., Geha, R.S., Hammarstrom, L., Nonoyama, S., Notarangelo, L.D., Ochs, H.D., Puck, J.M., Roifman, C.M., Seger, R., Tang, M.L.K., 2011. Primary immunodeficiency diseases: an update on the classification from the international union of immunological societies expert committee for primary immunodeficiency. Frontiers in Immunology 2, 54.

An, Y., Ohnishi, H., Matsui, E., Funato, M., Kato, Z., Teramoto, T., Kaneko, H., Kimura, T., Kubota, K., Kasahara, K., Kondo, N., 2011. Genetic variations in MyD88 adaptor-like are associated with atopic dermatitis. International Journal of Molecular Medicine 27, 795–801.

Andres, O., Strehl, K., Kölsch, U., Kunzmann, S., Lebrun, A.H., Stroh, T., Schwarz, K., Morbach, H., Bernuth, H.V., Liese, J., 2013. Even in pneumococcal sepsis CD62L shedding on granulocytes proves to be a reliable functional test for the diagnosis of interleukin-1 receptor associated kinase 4 deficiency. Pediatric Infectious Disease Journal 32, 1017–1019.

Bouma, G., Doffinger, R., Patel, S.Y., Peskett, E., Sinclair, J.C., Barcenas-Morales, G., Cerron-Gutierrez, L., Kumararatne, D.S., Davies, E.G., Thrasher, A.J., Burns, S.O., 2009. Impaired neutrophil migration and phagocytosis in IRAK-4 deficiency. British Journal of Haematology 147, 153–156.

Burns, K., Janssens, S., Brissoni, B., Olivos, N., Beyaert, R., Tschopp, J., 2003. Inhibition of interleukin 1 receptor/toll-like receptor signaling through the alternatively spliced, short form of MyD88 is due to its failure to recruit IRAK-4. Journal of Experimental Medicine 197, 263–268.

Cardenes, M., von Bernuth, H., Garcia-Saavedra, A., Santiago, E., Puel, A., Ku, C.L., Emile, J.F., Picard, C., Casanova, J.L., Colino, E., Bordes, A., Garfia, A., Rodriguez-Gallego, C., 2006. Autosomal recessive interleukin-1 receptor-associated kinase 4 deficiency in fourth-degree relatives. Journal of Pediatrics 148, 549–551.

Conway, D.H., Dara, J., Bagashev, A., Sullivan, K.E., 2010. Myeloid differentiation primary response gene 88 (MyD88) deficiency in a large kindred. Journal of Allergy and Clinical Immunology 126, 172–175.

Davidson, D.J., Currie, A.J., Bowdish, D.M.E., Brown, K.L., Rosenberger, C.M., Ma, R.C., Bylund, J., Campsall, P.A., Puel, A., Picard, C., Casanova, J.L., Turvey, S.E., Hancock, R.E.W., Devon, R.S., Speert, D.P., 2006. IRAK-4 mutation (Q293X): rapid detection and characterization of defective post-transcriptional TLR/IL-1R responses in human myeloid and non-myeloid cells. Journal of Immunology 177, 8202–8211.

de Beaucoudrey, L., Puel, A., Filipe-Santos, O., Cobat, A., Ghandil, P., Chrabieh, M., Feinberg, J., von Bernuth, H., Samarina, A., Janniere, L., Fieschi, C., Stephan, J.-L., Boileau, C., Lyonnet, S., Jondeau, G., Cormier-Daire, V., Le Merrer, M., Hoarau, C., Lebranchu, Y., Lortholary, O., Chandesris, M.-O., Tron, F., Gambineri, E., Bianchi, L., Rodriguez-Gallego, C., Zitnik, S.E., Vasconcelos, J., Guedes, M., Vitor, A.B., Marodi, L., Chapel, H., Reid, B., Roifman, C., Nadal, D., Reichenbach, J., Caragol, I., Garty, B.-Z., Dogu, F., Camcioglu, Y., Gulle, S., Sanal, O., Fischer, A., Abel, L., Stockinger, B., Picard, C., Casanova, J.-L., 2008. Mutations in STAT3 and IL12RB1 impair the development of human IL-17-producing T cells. Journal of Experimental Medicine 205, 1543–1550.

Delaglio, F., Grzesiek, S., Vuister, G., Zhu, G., Pfeifer, J., Bax, A., 1995. NMRPipe: a multidimensional spectral processing system based on UNIX pipes. Journal of Biomolecular NMR 6, 277–293.

Enders, A., Pannicke, U., Berner, R., Henneke, P., Radlinger, K., Schwarz, K., Ehl, S., 2004. Two siblings with lethal pneumococcal meningitis in a family with a mutation in interleukin-1 receptor-associated kinase 4. Journal of Pediatrics 145, 698–700.

Fukao, T., Kaneko, H., Birrell, G., Gatei, M., Tashita, H., Yoshida, T., Cross, S., Kedar, P., Watters, D., Khana, K.K., Misko, I., Kondo, N., Lavin, M.F., 1999. ATM is

upregulated during the mitogenic response in peripheral blood mononuclear cells. Blood 94, 1998–2006.
George, J., Kubarenko, A.V., Rautanen, A., Mills, T.C., Colak, E., Kempf, T., Hill, A.V.S., Nieters, A., Weber, A.N.R., 2010. MyD88 adaptor-like D96N is a naturally occurring loss-of-function variant of TIRAP. Journal of Immunology 184, 3025–3032.
George, J., Motshwene, P.G., Wang, H., Kubarenko, A.V., Rautanen, A., Mills, T.C., Hill, A.V.S., Gay, N.J., Weber, A.N.R., 2011. Two human MyD88 variants, S34Y and R98C, interfere with MyD88-IRAK4-Myddosome assembly. Journal of Biological Chemistry 286, 1341–1353.
Goddard, T.D., Kneller, D.G., 1999. SPARKY 3. University of California, San Francisco.
Hoarau, C., Gerard, B., Lescanne, E., Henry, D., Francois, S., Lacapere, J.J., El Benna, J., Dang, P.M.C., Grandchamp, B., Lebranchu, Y., Gougerot-Pocidalo, M.A., Elbim, C., 2007. TLR9 activation induces normal neutrophil responses in a child with IRAK-4 deficiency: involvement of the direct PI3K pathway. Journal of Immunology 179, 4754–4765.
Jiang, Z., Georgel, P., Li, C., Choe, J., Crozat, K., Rutschmann, S., Du, X., Bigby, T., Mudd, S., Sovath, S., Wilson, I.A., Olson, A., Beutler, B., 2006. Details of Toll-like receptor: adapter interaction revealed by germ-line mutagenesis. Proceedings of the National Academy of Sciences of the United States of America 103, 10961–10966.
Kato, Z., Jee, J., Shikano, H., Mishima, M., Ohki, I., Ohnishi, H., Li, A.L., Hashimoto, K., Matsukuma, E., Omoya, K., Yamamoto, Y., Yoneda, T., Hara, T., Kondo, N., Shirakawa, M., 2003. The structure and binding mode of interleukin-18. Nature Structural Biology 10, 966–971.
Krause, J.C., Ghandil, P., Chrabieh, M., Casanova, J.L., Picard, C., Puel, A., Creech, C.B., 2009. Very late-onset group B Streptococcus meningitis, sepsis, and systemic shigellosis due to interleukin-1 receptor-associated kinase-4 deficiency. Clinical Infectious Diseases 49, 1393–1396.
Ku, C.L., von Bernuth, H., Picard, C., Zhang, S.Y., Chang, H.H., Yang, K., Chrabieh, M., Issekutz, A.C., Cunningham, C.K., Gallin, J., Holland, S.M., Roifman, C., Ehl, S., Smart, J., Tang, M., Barrat, F.J., Levy, O., McDonald, D., Day-Good, N.K., Miller, R., Takada, H., Hara, T., Al-Hajjar, S., Al-Ghonaium, A., Speert, D., Sanlaville, D., Li, X.X., Geissmann, F., Vivier, E., Marodi, L., Garty, B.Z., Chapel, H., Rodriguez-Gallego, C., Bossuyt, X., Abel, L., Puel, A., Casanova, J.L., 2007. Selective predisposition to bacterial infections in IRAK-4-deficient children: IRAK-4-dependent TLRs are otherwise redundant in protective immunity. Journal of Experimental Medicine 204, 2407–2422.
Li, A.L., Kato, Z., Ohnishi, H., Hashimoto, K., Matsukuma, E., Omoya, K., Yamamoto, Y., Kondo, N., 2003. Optimized gene synthesis and high expression of human interleukin-18. Protein Expression and Purification 32, 110–118.
Lin, S.C., Lo, Y.C., Wu, H., 2010. Helical assembly in the MyD88-IRAK4-IRAK2 complex in TLR/IL-1R signalling. Nature 465, 885–890.
Loiarro, M., Gallo, G., Fanto, N., De Santis, R., Carminati, P., Ruggiero, V., Sette, C., 2009. Identification of critical residues of the MyD88 death domain involved in the recruitment of downstream kinases. Journal of Biological Chemistry 284, 28093–28103.
Lye, E., Mirtsos, C., Suzuki, N., Suzuki, S., Yeh, W.C., 2004. The role of interleukin 1 receptor-associated kinase-4 (IRAK-4) kinase activity in IRAK-4-mediated signaling. Journal of Biological Chemistry 279, 40653–40658.
Medvedev, A.E., Lentschat, A., Kuhns, D.B., Blanco, J.C.G., Salkowski, C., Zhang, S.L., Arditi, M.H., Gallin, J.I., Vogel, S.N., 2003. Distinct mutations in IRAK-4 confer hyporesponsiveness to lipopolysaccharide and interleukin-1 in a patient with recurrent bacterial infections. Journal of Experimental Medicine 198, 521–531.
Medvedev, A.E., Thomas, K., Awomoyi, A., Kuhns, D.B., Gallin, J.I., Li, X.X., Vogel, S.N., 2005. Cutting edge: expression of IL-1 receptor-associated kinase-4 (IRAK-4) proteins with mutations identified in a patient with recurrent bacterial infections alters normal IRAK-4 interaction with components of the IL-1 receptor complex. Journal of Immunology 174, 6587–6591.
Motshwene, P.G., Moncrieffe, M.C., Grossmann, J.G., Kao, C., Ayaluru, M., Sandercock, A.M., Robinson, C.V., Latz, E., Gay, N.J., 2009. An oligomeric signaling platform formed by the Toll-like receptor signal transducers MyD88 and IRAK-4. Journal of Biological Chemistry 284, 25404–25411.
Nada, M., Ohnishi, H., Tochio, H., Kato, Z., Kimura, T., Kubota, K., Yamamoto, T., Kamatari, Y.O., Tsutsumi, N., Shirakawa, M., Kondo, N., 2012. Molecular analysis of the binding mode of Toll/interleukin-1 receptor (TIR) domain proteins during TLR2 signaling. Molecular Immunology 52, 108–116.
Nagpal, K., Plantinga, T.S., Sirois, C.M., Monks, B.G., Latz, E., Netea, M.G., Golenbock, D.T., 2011. Natural loss-of-function mutation of myeloid differentiation protein 88 disrupts its ability to form Myddosomes. The Journal of Biological Chemistry 286, 11875–11882.
Nagpal, K., Plantinga, T.S., Wong, J., Monks, B.G., Gay, N.J., Netea, M.G., Fitzgerald, K.A., Golenbock, D.T., 2009. A TIR domain variant of MyD88 adapter-like (Mal)/TIRAP results in loss of MyD88 binding and reduced TLR2/TLR4 signaling. Journal of Biological Chemistry 284, 25742–25748.
Ohnishi, H., Miyata, R., Suzuki, T., Nose, T., Kubota, K., Kato, Z., Kaneko, H., Kondo, N., 2012a. A rapid screening method to detect autosomal-dominant ectodermal dysplasia with immune deficiency syndrome. Journal of Allergy and Clinical Immunology 129, 578–580.
Ohnishi, H., Tochio, H., Kato, Z., Kawamoto, N., Kimura, T., Kubota, K., Yamamoto, T., Funasaka, T., Nakano, H., Wong, R.W., Shirakawa, M., Kondo, N., 2012b. TRAM is involved in IL-18 signaling and functions as a sorting adaptor for MyD88. PLoS ONE 7, e38423.
Ohnishi, H., Tochio, H., Kato, Z., Orii, K.E., Li, A., Kimura, T., Hiroaki, H., Kondo, N., Shirakawa, M., 2009. Structural basis for the multiple interactions of the MyD88 TIR domain in TLR4 signaling. Proceedings of the National Academy of Sciences of the United States of America 106, 10260–10265.
Picard, C., Casanova, J.L., Puel, A., 2011. Infectious diseases in patients with IRAK-4, MyD88, NEMO, or I kappa B alpha deficiency. Clinical Microbiology Reviews 24, 490–497.
Picard, C., Puel, A., Bonnet, M., Ku, C.L., Bustamante, J., Yang, K., Soudais, C., Dupuis, S., Feinberg, J., Fieschi, C., Elbim, C., Hitchcock, R., Lammas, D., Davies, G., Al-Ghonaium, A., Al-Rayes, H., Al-Jumaah, S., Al-Hajjar, S., Al-Mohsen, I.Z., Frayha, H.H., Rucker, R., Hawn, T.R., Aderem, A., Tufenkeji, H., Haraguchi, S., Day, N.K., Good, R.A., Gougerot-Pocidalo, M.A., Ozinsky, A., Casanova, J.L., 2003. Pyogenic bacterial infections in humans with IRAK-4 deficiency. Science 299, 2076–2079.
Picard, C., von Bernuth, H., Ghandil, P., Chrabieh, M., Levy, O., Arkwright, P.D., McDonald, D., Geha, R.S., Takada, H., Krause, J.C., Creech, C.B., Ku, C.L., Ehl, S., Marodi, L., Al-Muhsen, S., Al-Hajjar, S., Al-Ghonaium, A., Day-Good, N.K., Holland, S.M., Gallin, J.I., Chapel, H., Speert, D.P., Rodriguez-Gallego, C., Colino, E., Garty, B.Z., Roifman, C., Hara, T., Yoshikawa, H., Nonoyama, S., Domachowske, J., Issekutz, A.C., Tang, M., Smart, J., Zitnik, S.E., Hoarau, C., Kumararatne, D.S., Thrasher, A.J., Davies, E.G., Bethune, C., Sirvent, N., de Ricaud, D., Camcioglu, Y., Vasconcelos, J., Guedes, M., Vitor, A.B., Rodrigo, C., Almazan, F., Mendez, M., Arostegui, J.I., Alsina, L., Fortuny, C., Reichenbach, J., Verbsky, J.W., Bossuyt, X., Doffinger, R., Abel, L., Puel, A., Casanova, J.L., 2010. Clinical features and outcome of patients with IRAK-4 and MyD88 deficiency. Medicine 89, 403–425.
Qin, J.Z., Jiang, Z.F., Qian, Y.C., Casanova, J.L., Li, X.X., 2004. IRAK4 kinase activity is redundant for interleukin-1 (IL-1) receptor-associated kinase phosphorylation and IL-1 responsiveness. Journal of Biological Chemistry 279, 26748–26753.
Suzuki, N., Suzuki, S., Duncan, G.S., Millar, D.G., Wada, T., Mirtsos, C., Takada, H., Wakeham, A., Itie, A., Li, S.Y., Penninger, J.M., Wesche, H., Ohashi, P.S., Mak, T.W., Yeh, W.C., 2002. Severe impairment of interleukin-1 and Toll-like receptor signalling in mice lacking IRAK-4. Nature 416, 750–754.
Takada, H., Yoshikawa, H., Imaizumi, M., Kitamura, T., Takeyama, J., Kumaki, S., Nomura, A., Hara, T., 2006. Delayed separation of the umbilical cord in two siblings with interleukin-1 receptor-associated kinase 4 deficiency: rapid screening by flow cytometer. Journal of Pediatrics 148, 546–548.
von Bernuth, H., Ku, C.-L., Rodriguez-Gallego, C., Zhang, S., Garty, B.-Z., Marodi, L., Chapel, H., Chrabieh, M., Miller, R.L., Picard, C., Puel, A., Casanova, J.-L., 2006. A fast procedure for the detection of defects in toll-like receptor signaling. Pediatrics 118, 2498–2503.
von Bernuth, H., Picard, C., Jin, Z., Pankla, R., Xiao, H., Ku, C.-L., Chrabieh, M., Ben Mustapha, I., Ghandil, P., Camcioglu, Y., Vasconcelos, J., Sirvent, N., Guedes, M., Vitor, A.B., Herrero-Mata, M.J., Arostegui, J.I., Rodrigo, C., Alsina, L., Ruiz-Ortiz, E., Juan, M., Fortuny, C., Yague, J., Anton, J., Pascal, M., Chang, H.-H., Janniere, L., Rose, Y., Garty, B.-Z., Chapel, H., Issekutz, A., Marodi, L., Rodriguez-Gallego, C., Banchereau, J., Abel, L., Li, X., Chaussabel, D., Puel, A., Casanova, J.-L., 2008. Pyogenic bacterial infections in humans with MyD88 deficiency. Science 321, 691–696.
Wang, D., Zhang, S., Li, L., Liu, X., Mei, K., Wang, X., 2010. Structural insights into the assembly and activation of IL-1 beta with its receptors. Nature Immunology 11, 905–911.
Weller, S., Bonnet, M., Delagreverie, H., Israel, L., Chrabieh, M., Maródi, L., Rodriguez-Gallego, C., Garty, B.Z., Roifman, C., Issekutz, A.C., Zitnik, S.E., Hoarau, C., Camcioglu, Y., Vasconcelos, J., Rodrigo, C., Arkwright, P.D., Cerutti, A., Mefre, E., Zhang, S.Y., Alcais, A., Puel, A., Casanova, J.L., Picard, C., Weill, J.C., Reynaud, C.A., 2012. IgM+IgD+CD27+ B cells are markedly reduced in IRAK-4–, MyD88– and TIRAP– but not UNC-93B-deficient patients. Blood 120, 4992–5001.
Yoshikawa, H., Watanabe, S., Imaizumi, M., 2010. Successful prevention of severe infection in Japanese siblings with interleukin-1 receptor-associated kinase 4 deficiency. Journal of Pediatrics 156, 168.

Transfusion and Apheresis Science 49 (2013) 504–506

Contents lists available at SciVerse ScienceDirect

Transfusion and Apheresis Science

journal homepage: www.elsevier.com/locate/transci

Case Report

Peripheral blood stem cell transplantation in a significant body weight difference between a smaller donor and a larger recipient: A case report

Michinori Funato [a,*], Hideo Kaneko [b], Hideo Sasai [a], Kazuo Kubota [a], Michio Ozeki [a], Kaori Kanda [a], Zenichiro Kato [a], Naomi Kondo [a]

[a] Department of Pediatrics, Graduate School of Medicine, Gifu University, 1-1 Yanagido, Gifu 501-1194, Japan
[b] Department of Clinical Research, National Hospital Organization, Nagara Medical Center, 1300-7 Nagara, Gifu 502-8558, Japan

ARTICLE INFO

Article history:
Received 3 June 2012
Received in revised form 27 September 2012
Accepted 10 January 2013

Keywords:
Peripheral blood stem cell transplantation
Peripheral blood stem cell collection
Benefits of younger donors
Significant body weight difference
Safety of donors

ABSTRACT

Allogeneic peripheral blood stem cell transplantation (PBSCT) is becoming a common transplantation procedure in children. However, few benefits have been reported, in particular in regard to the choice of small children as donors for larger recipients. We report a case of relapsed acute myeloid leukemia (body weight 52 kg and blood type O) who underwent allogeneic PBSCT from his smaller human leukocyte antigen-matched brother (body weight 29.9 kg and blood type A).

1. Introduction

Since the report by Thomas et al. in 1957 [1], bone marrow (BM) aspirated from the iliac crest was the main source of hematopoietic stem cells for transplantation [2], and peripheral blood (PB) stem cells totally replaced aspirated BM in autologous stem cell transplantation (SCT) during the 1990s. In allogeneic SCT, a similar trend has been seen during the last decade for patients with hematological malignancies [2]. Also, cord blood (CB) can presently be used as a stem cell source for allogeneic SCT. Each has its own benefits and risks, therefore clinicians have made a choice from three sources of hematopoietic stem cells including BM, PB, and CB, on the basis of disease of recipient, condition of donor and recipient, safety of donor, and so on.

At present, approximately 100% of autologous SCT and 75% of allogeneic SCT, instead of BM, are performed using PB in adult [3]. The use of PB stem cells has been reported to result in faster engraftment and the graft-versus-leukemia (GVL) effect correlated with chronic graft-versus-host disease (GVHD) [2,4]. In addition, recovery time for PB donors is shorter than that for BM donors [5].

Similarly, in children, the use of PB stem cells tends to increase for not only autologous but also for allogeneic peripheral blood stem cell transplantation (PBSCT), and with this, the number of normal pediatric donors has also been increasing, of which many are siblings [6]. In general, younger donors in PBSCT need two large venous catheters and have both short-term and long-term risk from granulocyte colony-stimulating factor (G-CSF) mobilization treatment, and also have increased risks of bleeding due to apheresis and thrombocytopenia, which occasionally expose to further risks of allogeneic blood products [4,6]. Few benefits of younger donors in PBSCT have been

* Corresponding author. Tel.: +81 58 2306386; fax: +81 58 2306387.
E-mail address: mfunato@me.com (M. Funato).

1473-0502/$ - see front matter © 2013 Elsevier Ltd. All rights reserved.
http://dx.doi.org/10.1016/j.transci.2013.01.015

reported, in particular in regard to the choice of small children who may be considered as potential donors for larger recipients. Herein, we describe a patient with relapsed acute myeloid leukemia (AML) who underwent allogeneic PBSCT from his smaller human leukocyte antigen (HLA)-matched brother.

2. Case report

A 13-year-old boy was referred to Gifu University Hospital because of an ache in his bilateral hip. On admission, his physical examination showed cervical lymphadenopathy, but no hepatosplenomegaly and purpura were evident. Laboratory examination revealed a white blood cell count of 6400/μl with 69.5% blasts, 6.5% neutrophils, and 22.5% lymphocytes, a hemoglobin concentration of 10.9 g/dl, and a platelet count of 89,000/μl. BM examination confirmed the diagnosis of AML (FAB M5) with 95.8% blasts. Cytogenetic analysis of the BM cells revealed 48, XY, +8, +8, t(11;19)(q23;p13.3) [12]/46, XY [8], and flow cytometric immunophenotyping in the blast cells was positive for CD15, CD33, CD64, CD65, and HLA-DR. Reverse-transcription polymerase chain reaction showed gene rearrangement of *MLL/ENL*, and fluorescence in situ hybridization analysis using the *MLL* probe showed the typical split-signal pattern. He had multiagent-chemotherapy according to the Japan Association of Childhood Leukemia Study AML99 protocol, consisting of etoposide, cytosine arabinoside, mitoxantrone, and idarubicin. Two months later, he achieved complete remission (CR) and received 4 chemotherapy courses as consolidation.

However, he had a relapse at age 16 years. BM examination revealed the same myeloblasts. After he achieved his second CR, he was scheduled to undergo allogeneic SCT from his HLA-matched brother, a 10-year-old boy. But there was difficulty with the significant body weight difference between the larger patient (body weight 52 kg) and the smaller related donor (body weight 29.9 kg), and with the incompatible blood type between the patient (blood type O) and the related donor (blood type A). To collect $4–6 \times 10^6$ CD34 positive cells/kg of recipient weight, and further to expect a GVL effect for our patient with the malignant disorder, we chose PBSCT. The related donor received G-CSF treatment with 5 daily injections, and his platelet count had fallen to 80,000/μl without any other complications. We obtained 7.0×10^8 nucleated cells/kg of recipient weight (4.07×10^6 CD34 positive cells/kg of recipient weight) after removal of red blood cells. Then, we treated him with a conditioning regimen consisting of busulfan (0.8 mg/kg/day, 4 days) and melphalan (60 mg/m^2/day, 3 days). Short-term methotrexate and cyclosporine were used as GVHD prophylaxis. Hematological reconstitution revealed a neutrophil count of more than 500/μl on day 11, reticulocytes of more than 10% on day 15, and a platelet count of more than 50,000/μl on day 34. BM examination on day 84 demonstrated complete chimerism by short tandem repeat analysis, and he had no complications except the development of grade I acute GVHD (skin, stage 1) on day 13. He is now at 3 years after PBSCT, with no local or systemic signs of disease recurrence.

3. Discussion

It has been 25 years since PBSCT was introduced as a transplant modality [3]. In the 1950s, circulating hematopoietic stem cells in PB were discovered, followed by the development of continuous-flow apheresis technology in the early 1960s and its first clinical application in the early 1970s. In the late 1970s to the early 1980s, clinical PBSCT attempts failed, but successful PBSCT was reported in a patient with Burkitt lymphoma in 1986 [7]. In the late 1980s, the molecular cloning and clinical development of G-CSF advanced clinical PBSCT. In addition, small-molecule CXCR4 antagonist for stem cell mobilization was developed in the early 2000s. At present, PBSCT is the most common transplantation procedure performed in medicine [3]. Herein, we described a patient with relapsed AML who underwent allogeneic PBSCT from his HLA-matched brother, even though there was a significant body weight difference between the two.

AML in our patient relapsed, but he fortunately had an HLA-matched sibling as the transplant-donor. This is generally preferred by clinicians because of reduced risks of GVHD and other transplant-related complications. So, we had to arrange an SCT for his relapsed AML, but there was the problem of significant body weight difference between the two and also incompatible blood type. Recently, the efficacy and safety of allogeneic PB stem cell collection in children was reported and this study showed that the mean number of CD34 positive cells/kg of donor weight was 9.1×10^6 in normal pediatric donors of PB stem cells that received an average of 4 days of G-CSF and an average of 1.4 apheresis [6]. On the other hand, it was reported that mean collection yield in healthy pediatric donors of BM single harvest was 4.78×10^6 CD34 positive cells/kg of donor weight [8]. In our patient, this was the estimated collection capability of 5.23×10^6 CD34 positive cells/kg of recipient weight in PB and 2.74×10^6 CD34 positive cells/kg of recipient weight in BM. To collect an adequate number of CD34 positive stem cells, that is $4–6 \times 10^6$ CD34 positive cells/kg of recipient weight [9], we informed both the donor and the recipient of the medical and psychosocial benefits and risks of PBSCT and PB stem cell collection, and they then underwent PB stem cell collection in 2 apheresis after 5 days of G-CSF treatment with their consent. As a result, we obtained 4.07×10^6 CD34 positive cells/kg of recipient weight for SCT after removal of red blood cells, and this led to successful PBSCT in our patient.

Some medical and psychosocial risks in PBSCT and PB stem cell collection have been reported [4]. In particular, although most G-CSF effects in healthy donor are thought to be transient and selflimited, preliminary data suggest that G-CSF affects not only myeloid cells but also chromosomal integrity and gene expression [10]. In addition, there is the theoretical danger of potentially increasing the long-term risk of leukemia [10]. Our donor did not develop any severe complications except mild thrombocytopenia during stem-cell mobilization treatment and collection, and is now followed up for 3 years, with no local or systemic signs. Moreover, we could care ethically for both our

patient and donor, and it greatly influenced successful PBSCT.

In conclusion, we reported a significant case of relapsed AML who underwent PBCST having a significant body weight difference with a smaller donor. This case illustrates the importance of small children who may be considered as potential donors for larger recipients in SCT. However, the safety limit for body weight difference between small donors and larger recipients needs to be investigated.

4. Conflict of interest

The authors state no conflict of interest.

Acknowledgments

This study was supported in part by Health and Labor Sciences Research Grants of Research on Measures for Intractable Diseases from the Ministry of Health, Labor and Welfare.

References

[1] Thomas ED, Lochte Jr HL, Lu WC, Ferrebee JW. Intravenous infusion of bone marrow in patients receiving radiation and chemotherapy. N Engl J Med 1957;257:491–6.
[2] Aschan J. Allogeneic haematopoietic stem cell transplantation: current status and future outlook. Br Med Bull 2006;77–78:23–36.
[3] Körbling M, Freireich EJ. Twenty-five years of peripheral blood stem cell transplantation. Blood 2011;117:6411–6.
[4] American academy of pediatrics. Committee on bioethics. Children as hematopoietic stem cell donors. Pediatrics 2010;125:392–404.
[5] Bredeson C, Leger C, Couban S, Simpson D, Huebsch L, Walker I, et al. An evaluation of the donor experience in the canadian multicenter randomized trial of bone marrow versus peripheral blood allografting. Biol Blood Marrow Transplant 2004;10:405–14.
[6] Pulsipher MA, Levine JE, Hayashi RJ, Chan KW, Anderson P, Duerst R, et al. Safety and efficacy of allogeneic PBSC collection in normal pediatric donors: the pediatric blood and marrow transplant consortium experience (PBMTC) 1996–2003. Bone Marrow Transpl 2005;35:361–7.
[7] Körbling M, Dörken B, Ho AD, Pezzutto A, Hunstein W, Fliedner TM. Autologous transplantation of blood-derived hemopoietic stem cells after myeloablative therapy in a patient with Burkitt's lymphoma. Blood 1986;67:529–32.
[8] Biral E, Chiesa R, Cappelli B, Roccia T, Frugnoli I, Noè A, et al. Multiple BM harvests in pediatric donors for thalassemic siblings: safety, efficacy and ethical issues. Bone Marrow Transpl 2008;42:379–84.
[9] Leung AY, Kwong YL. Haematopoietic stem cell transplantation: current concepts and novel therapeutic strategies. Br Med Bull 2010;93:85–103.
[10] Anderlini P, Champlin RE. Biologic and molecular effects of granulocyte colony-stimulating factor in healthy individuals: recent findings and current challenges. Blood 2008;111:1767–72.

Copyedited by: AS

International Immunology
doi:10.1093/intimm/dxt072

Open conformation of WASP regulates its nuclear localization and gene transcription in myeloid cells

Chung Yeng Looi[1], Yoji Sasahara[1], Yuko Watanabe[1], Miki Satoh[1], Ikuko Hakozaki[1], Meri Ouchi[1], Won Fen Wong[2], Wei Du[3], Toru Uchiyama[1], Satoru Kumaki[1], Shigeru Tsuchiya[1] and **Shigeo Kure[1]**

[1]Department of Pediatrics, Tohoku University Graduate School of Medicine, Sendai, Miyagi 980-8574, Japan
[2]Department of Molecular Immunology, Institute of Development, Aging and Cancer, Tohoku University, Sendai, Miyagi 980-8575, Japan
[3]Division of Experimental Hematology, Cincinnati Children's Hospital Medical Center, Cincinnati, OH 45229, USA

Correspondence to: Y. Sasahara, Department of Pediatrics, Tohoku University Graduate School of Medicine, 1-1 Seiryou-machi, Aoba-ku, Sendai, Miyagi 980-8574, Japan. E-mail: ysasahara@med.tohoku.ac.jp

Received 10 March 2012, *accepted* 17 December 2013

Abstract

Wiskott–Aldrich syndrome protein (WASP) is a responsible gene mutated in Wiskott–Aldrich syndrome and a major actin regulator in the cytoplasm. Although rare gain-of-function mutations in the WASP gene are known to result in X-linked neutropenia (XLN), molecular pathogenesis of XLN is not fully understood. In this study, we showed that all reported constitutively activating mutants (L270P, S272P and I294T) of WASP were hyperphosphorylated by Src family tyrosine kinases and demonstrated higher actin polymerization activities compared with wild-type (WT) WASP. Further analysis showed a tendency of activating WASP mutants to localize in the nucleus compared with WT or Y291F mutant of WASP. In addition, we found that WASP could form a complex with nuclear RNA-binding protein, 54 kDa and RNA polymerase II (RNAP II). Chromatin immunoprecipitation (ChIP) assay revealed that WASP associated with DNA, although the affinity was relatively weaker than RNAP II. To determine whether gene transcription was affected by WASP mutation in myeloid cells, we performed microarray analysis and found different expression profiles between WT and L270P WASP-transfected K562 cells. Among the genes affected, granulocyte colony-stimulating factor receptor, Runx1, and protein tyrosine phosphatase receptor c were included. ChIP on chip analysis of genomic DNA showed WT and L270P WASP had highly similar DNA binding pattern but differed in binding affinity at the same locus. Therefore, our results suggest that open conformation of WASP regulates its nuclear localization and plays requisite roles in regulating gene transcription that would contribute to the outcome of myeloid cells in the nucleus.

Keywords: RNA polymerase II, Wiskott–Aldrich syndrome protein, X-linked neutropenia

Introduction

Wiskott–Aldrich syndrome (WAS) is an X-linked recessive immunodeficiency characterized by thrombocytopenia, eczema and recurrent infections (1). Gene encoding Wiskott–Aldrich syndrome protein (WASP) was first discovered in 1994 as the defective gene product leading to WAS through linkage analysis (2). WASP is exclusively expressed in hematopoietic cells (3). The loss-of-function mutations in the WASP gene are commonly found in patients with classical WAS and milder variant X-linked thrombocytopenia. The gain-of-function mutations in the WASP gene are rare and responsible for X-linked neutropenia (XLN) (4–6). Although three known activating WASP mutations (L270P, S272P and I294T) have been reported, molecular pathogenesis of XLN has not been clearly understood.

WASP is a key molecule that mediates signals to regulate actin polymerization through its carboxyl terminus consisting of verprolin, cofilin and acidic (VCA) domain (7). The VCA region binds to actin-related protein 2/3 (Arp2/3) complex and recruits monomeric actin to stimulate nucleation of branched actin filaments (8). WASP is implicated in the control of actin dynamics, which is important for cellular processes such as chemotaxis, phagocytosis, cell–cell contact in hematopoietic cells (9). WAS phenotype is characterized by abnormal actin structures in platelets and immune cells (10, 11). For example, murine cells deficient in WASP are unable to cap CD3 due to defective actin reorganization in response to T-cell receptor signaling (12–14). WASP null peripheral blood monocytes and macrophages exhibit impaired FcγR-mediated phagocytosis

(15). On the other hand, exposure of VCA domain due to constitutively activating WASP mutation leads to enhanced actin polymerization activities in cells. The aberrant actin polymerization has been shown to affect cytokinesis of cells and induced genomic instability in lymphocytes (6, 16).

WASP is self-regulated by the adoption of an autoinhibited conformation through hydrophobic interaction between VCA domain and the GTPase-binding domain (GBD, residue 230–288). Binding of Cdc42-GTP to the GBD disrupts this closed conformation and releases the C-terminal to interact with Arp2/3 complex (17). Mutations in the GBD were reported to inhibit formation of closed conformation leading to constitutively activation of WASP in cells. WASP can also be activated through phosphorylation of tyrosine 291 (Y291). Y291 of WASP is a consensus site phosphorylated by Src family tyrosine kinases. Phosphorylation of Y291 WASP has functional relevance in transmitting signals independent of its actin polymerization role in cells. For example, a study showed that IL-2 production in T cells after CD3 stimulation was normal in a WASP mutant with deleted VCA domain (18). To avoid uncontrolled phosphorylation by tyrosine kinases, the Y291 is buried deep in the autoinhibited domain of WASP and phosphorylation efficiency of Y291 is low in the absence of activation signals such as Cdc42-GTP binding (19, 20). So far, the phosphorylation profiles of Y291 of activating WASP mutants are unknown and remained to be investigated.

A number of proteins such as neuronal-WASP (N-WASP) and Wiskott–Aldrich syndrome protein verprolin-homologous protein (WAVE) shuttle between nucleus and cytoplasm (21, 22). N-WASP is a member of WASP family proteins, which has >50% homology to WASP over the full length (23). Recently, N-WASP has been shown to affect gene transcription through binding to the complex of nuclear RNA-binding protein, 54 kDa (p54nrb) and RNA polymerase II (RNAP II) (24). Interestingly, WASP has been discovered to play a role in T_h1 differentiation by regulating expressions of several master genes (25).

In this study, we showed that constitutively activating mutants of WASP were hyperphosphorylated by Src family tyrosine kinases and activating WASP mutants had higher tendency to localize in the nucleus. In addition, both wild-type (WT) and L270P WASP formed a complex with p54nrb, RNAP II and DNA, suggesting a role in gene transcription. Since active forms of WASP have been shown to affect myeloid cells, we established K562 clones stably expressing WT or L270P WASP. Through microarray and chromatin immunoprecipitation (ChIP) on chip analysis, we found different gene expression profiles and different binding affinity at the same locus between WT and L270P WASP, suggesting significant roles of WASP in regulating gene transcription in myeloid cells.

Methods

Antibodies, plasmids and WASP mutagenesis

Anti-p54nrb, anti-Lck, anti-Fyn and anti-vinculin antibodies were from Santa Cruz Biotechnology (Santa Cruz, CA, USA). Anti-WASP (5A5) was from BD Biosciences (San Jose, CA, USA). Anti-phosphotyrosine (4G10) and anti-RNAP II antibodies were from Upstate (Lake Placid, NY, USA). Anti-β-actin was from Sigma (St Louis, MO, USA). Anti-Dsred, anti-GFP and anti-hemagglutinin (HA) were purchased from Clontech. HRP-conjugated secondary antibodies were from Amersham Biosciences (Piscataway, NJ, USA). FITC-conjugated anti-human CD45, PE-conjugated anti-human G-CSFR and control rabbit polyclonal IgG antibody were from R&D Systems (Minneapolis, MN, USA). pEGFP-WT or Y291F WASP expression vectors were gifts by K. A. Siminovitch (University of Toronto). The mutations L270P, S272P and I294T were introduced using QuikChange site-directed mutagenesis kit (Stratagene, Amsterdam, The Netherlands) into pEGFP-WT WASP template. Primers for L270P: 5′-CAGATCTGCGGAGTCCGTTCTCCAGGGCAGG-3′ and 5′-CCTGCCCTGAGAACGGACTCCGCAGATCTG-3′, S272P: 5′-CTGCGGAGTCTGTTCCCCAGGGCAGGAATCAGC-3′ and 5′-GCTGATTCCTGCCCTGGGGAACAGACTCCGCAG-3′, I294T: 5′-CTTATCTACGACTTCACTGAGGACCAGGGTGGG-3′ and 5′-CCCACCCTGGTCCTCAGTGAAGTCGTAGATA AG-3′ were used. All constructs were verified by sequencing. HA-tagged WT WASP and L270P WASP plasmids were prepared from pEGFP-WASP constructs. pME-Lck and pCXN2-Fyn vectors were provided by M. Satake and N. Ishii (Tohoku University), respectively. pEGFP and pDsred vectors were from Clontech (Mountain View, CA, USA). p54nrb was PCR amplified using cDNA from Hela cells and the final product was inserted in-frame into pDsred vector.

Cell culture and transient transfection

K562 and COS-7 cells were maintained in RPMI and DMEM medium, respectively, supplemented with 10% FCS.

2×10^5 COS-7 cells per well were seeded into 6-well plates. After 12 h, cells were transfected with 1-μg respective plasmids using Lipofectamine LTX with Plus reagent according to the manufacturer's instructions (Invitrogen, Carlsbad, CA, USA). Cells were lysed with lysis buffer or fixed with 4% paraformaldehyde at 24 h after transfection.

Establishment of K562 cells stably expressing WT or L270P WASP

EGFP- or HA-tagged WASP plasmids were transfected by electroporation into 2×10^6 K562 cells using Gene Pulser II (Bio-Rad, Hercules, CA. USA) at 280 V, 500-mF. Transfected cells were plated into 96-well plates and selected with 500 μg ml^{-1} of geneticin (Gibco, Carlsbad, CA, USA) for 3 weeks. Several colonies stably expressing WT or L270P WASP were selected by western blotting using anti-WASP antibody. After confirming WASP expression, cells were subjected to limiting dilution in 96-well plates to obtain single cell colonies.

Immunoprecipitation and western blotting

Cells were lysed in lysis buffer containing 50 mM Tris (pH 7.4), 1% Triton X-100, 150 mM sodium chloride, 2 mM sodium orthovanadate, 5 mM EDTA, 1 mM phenylmethylsulfonyl fluoride and cocktail of protease inhibitors. Nuclear and cytoplasmic fractionation was performed essentially as described (21). Lysates were precleared with protein-G sepharose beads (Amersham Biosciences) before subjected to immunoprecipitation at 4°C for 1 h with anti-GFP antibody (2–μg). Immunoprecipitates were recovered by protein-G

sepharose beads. Proteins were resolved on 10% SDS–PAGE gels and transferred to polyvinylidine difluoride membranes. Membranes were probed with primary and corresponding secondary antibodies conjugated to HRP. Membranes were developed using enhanced chemiluminescence reagents (Amersham Biosciences).

Immunofluorescence microscopy

COS-7 cells were transfected with EGFP-tagged WT, L270P, S272P, I294T, Y291F WASP or HA-tagged WT, L270P WASP with or without Dsred-p54nrb. After 24 h, cells were washed twice with PBS before fixing with 4% (w/v) paraformaldehyde. Stained cells with anti-HA antibody were mounted on slides with ProLong Gold antifade reagent with 4,6-diamino-2-phenylindole (DAPI) (Invitrogen). Slides were observed using Olympus BX61 fluorescent microscope. Fluorescent intensities in the nucleus (F_n) and cytoplasm (F_c) of the cells were quantified in 50 transfected cells using the Lumina Vision software. The ratio of $F_c - F_n$ versus F_c was then calculated and used to quantify nuclear localization of WASP as described previously (21).

$$\text{Nuclear localization ratio} = \frac{F_c - F_n}{F_c}$$

Statistical analysis was performed by Student's *t*-test.

F-actin quantification

COS-7 cells were transfected with EGFP-tagged WT, L270P, S272P, I294T, Y291F WASP or EGFP expression vectors as described above. After 24 h, cells were collected and immediately fixed with 4% paraformaldehyde. Fixed cells were stained and permeabilized in a single step in buffer containing 0.1% Triton X-100 and phalloidin 568. Stained cells were thoroughly washed with PBS for five times and total F-actin content per EGFP intensities were measured by plate reader.

Microarray analysis

The expression levels of WT or L270P WASP in stably transfected K562 clones were examined by reverse transcription (RT)–PCR and western blotting. K562 clones expressing comparable WT or L270P WASP levels were selected. Total RNA was extracted from cells using RNeasy Mini Kit (Qiagen). Quality of RNA was determined using denaturing formaldehyde gel electrophoresis and Bioanalyser (BMR, Chiba, Japan), and concentration of each sample was measured by Nanodrop (LMS, Tokyo, Japan). A total of five samples were used for analysis, including K562 parental cell line (sample name K562), two samples of K562 WT WASP extracted at different time (sample name WT-1, WT-2) and two samples of K562 L270P WASP extracted at different time (sample name MUT-1, MUT-2). The experimental design includes initial pair comparison and subsequently pair to pair elimination using each sample as standard. The groupings were as follows: (i) **K562** versus WT-1, (ii) **K562** versus MUT-1, (iii) **K562** versus WT-2, (iv) **K562** versus MUT-2, (v) **WT-1** versus MUT-1, (vi) **WT-1** versus WT-2, (vii) **WT-1** versus MUT-2, (viii) **WT-2** versus MUT-2, (ix) **WT-2** versus MUT-1 and (x) **MUT-1** versus MUT-2 (bold letters indicated standard). GeneChipR Human Genome U133 Plus 2.0 Array (Affymetrix, Santa Clara, CA, USA) was used because this chip contains around 54000 probes, which covered most of the genes.

Data mining was performed using Agilent Genespring viewer software by the criteria of either up-regulated 2 times or down-regulated 0.5 times. Genes were narrowed down further by applying the following key words: apoptosis, differentiation, granulocyte and myeloid after comparison. Genes that overlapped in groups 5, 7, 8, and 9 were chosen and non-overlapping genes were further eliminated using Venn diagram. Candidate genes were selected and preceded to confirmation using RT–PCR and western blotting.

Reverse transcription–PCR

Total RNA isolated with RNeasy mini kit and DNase I (Qiagen) was applied to the column to remove DNA during RNA purification. After reverse transcription of 2 μg of total RNA by oligo-dT primer using SuperScript MMLV reverse transcriptase (Invitrogen), the resulting single-stranded cDNA was amplified using high fidelity PCR system (Toyobo). PCR was performed on 100 ng of single-stranded cDNA in the presence of 5 μM oligonucleotide primers in Takara Minidice Thermal Cycler (30 cycles, denaturing at 95°C for 1 min, annealing at 60°C for 30 s and extension at 68°C for 2 min). Aliquots of the amplified products were separated by 1.5% agarose gel electrophoresis, visualized by ethidium bromide staining and quantified by CS3 imager analyzer (ATTO, Tokyo, Japan). The primers used were as follows: G-CSFR: forward 5′-GCCACTGCTGCATCCCACGC-3′ and reverse 5′-GGAGTCTGGTCAGACTGGG-3′, PTPRC: forward 5′-CAGG CAGCAATGCTATCTCAG-3′ and reverse 5′-CTCCTG GACTCCCAAAATCTG-3′, Runx1: forward 5′-CCAGCAAGCTG AGGAGCGGCG-3′ and reverse 5′-TGACGGTGACCAGAG TG-3′.

Flowcytometry analysis

1×10^5 cells of K562 parental cell line, K562 clones stably transfected with WT or L270P WASP, were blocked with 0.5% BSA before staining with FITC-CD45, PE-G-CSFR or control IgG antibodies for 40 min at 4°C. Stained cells were washed twice with PBS before subjecting to flowcytometry analysis on FACS Calibur (Becton Dickinson, San Jose, CA, USA), and a total of 10000 events were collected.

ChIP assay

Chromatin of K562 clones stably transfected with WT or L270P WASP was fixed and immunoprecipitated with 2 μg anti-RNAP II, anti-WASP (5A5) or normal rabbit IgG by using ChIP assay kit (Upstate Cell Signaling Solutions, Charlottesville, VA, USA) as recommended by the manufacturer. After DNA purification, the presence of selected DNA sequences was further assessed by PCR. The primers used were as follows: GAPDH forward: 5′-TACTAGCGGTTTTACGGGCG-3′ and reverse: 5′-TCGAACAGGAGGAGCAGAGAGCGA-3′.

ChIP on chip analysis

Microarray hybridization was performed by the NimbleGen Service Facility in Tokyo. K562 cells expressing WT or L270P WASP were cross-linked with formaldehyde before subjecting

to sonication to shear DNA. Immunoprecipitation was performed with anti-WASP (5A5) antibody, and 100 ng of precipitated DNA was used for amplification using whole genome amplification kit (Sigma). Amplified DNA in each sample was labeled with Cy3 or Cy5 before hybridizing to Agilent Human Promoter 244K chip. Images were taken with Agilent DNA microarray scanner and the data were analyzed by Agilent's GeneSpring software.

Results

Characterization of constitutively activating WASP mutants

We constructed L270P, S272P and I294T WASP from pEGFP-WT WASP by PCR mutagenesis (Fig. 1A). Non-phosphorylated form of WASP (Y291F) was included as negative control of tyrosine phosphorylation (26). To examine whether they were functionally active, COS-7 cells were transfected with EGFP-tagged

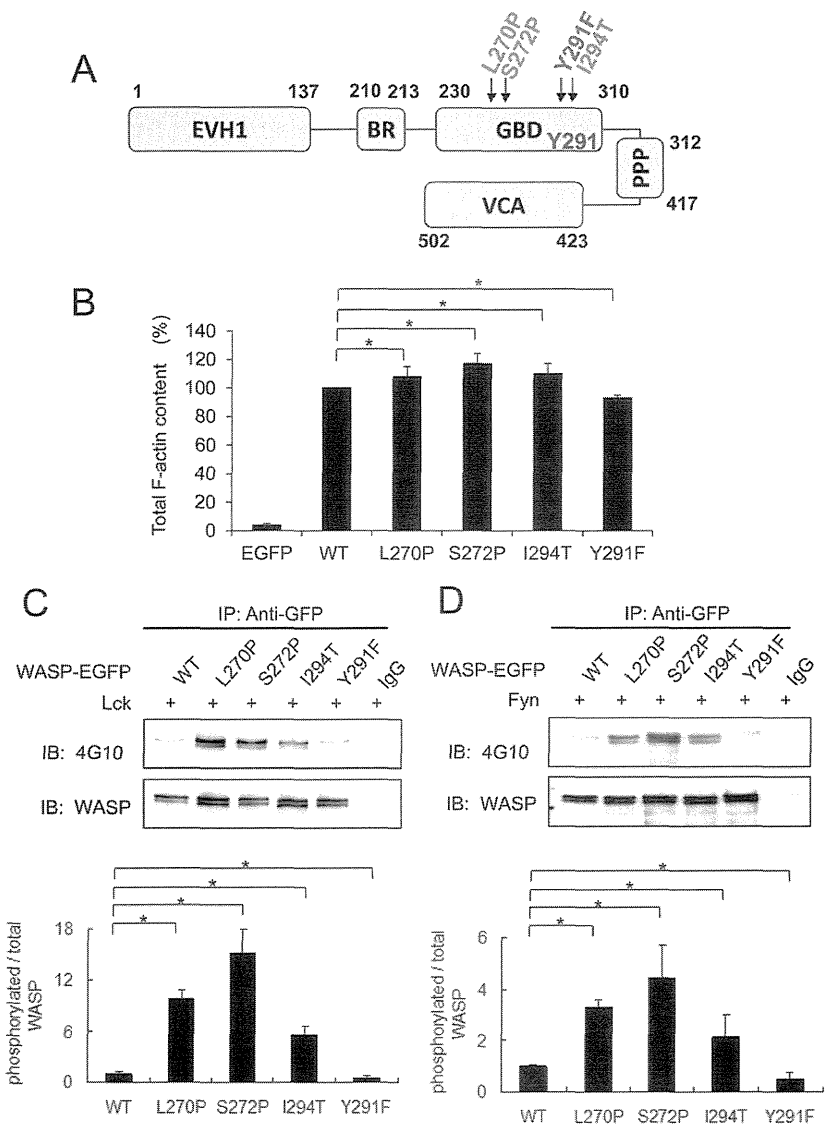

Fig. 1. Activating WASP mutants with open conformation are hyperphosphorylated by Src family tyrosine kinases and result in increased F-actin contents *in vivo*. (A) Location of Y291 (blue), L270P, S272P, I294T (red) and Y291F (green) in WASP. EVH1, Ena/Vasp homology 1; BR, basic region; PPP, polyproline rich domain. (B) COS-7 cells were transfected with EGFP-tagged WASP constructs. Means ± SDs of F-actin contents were shown in three independent experiments. (C and D) EGFP-tagged WASP constructs were co-transfected with Lck (C) or Fyn (D) expression vectors into COS-7 cells. Immunoprecipitates with anti-GFP or control IgG were probed with anti-phosphotyrosine 4G10 or anti-WASP antibody. Lower panels showed the relative increase of phosphorylated WASP in total amount of WASP compared with WT. Means ± SDs were shown in three independent experiments. Asterisks indicated statistically significant.

WASP constructs or EGFP alone. After 24 h, cells were fixed and stained with phalloidin 568. As shown in Fig. 1(B), constitutively activating WASP mutants (L270P, S272P and I294T) demonstrated significantly higher F-actin content than WT ($P < 0.01$), while Y291F showed decreased F-actin content ($P < 0.01$).

Torres and Rosen (19, 20) showed that close conformation of WASP is crucial to prevent Y291 phosphorylation by Src family tyrosine kinase. To examine whether activating WASP mutants were susceptible to enhanced tyrosine phosphorylation, we co-transfected Lck or Fyn with WASP expression plasmids into COS-7 cells. After 24 h, cells were harvested and total lysates were immunoprecipitated with anti-GFP or control IgG antibody. The intensities of bands probed with anti-phosphotyrosine and anti-WASP antibody were quantified by densitometry analysis. Tyrosine phosphorylation levels of activating L270P, S272P or I294T WASP mutants by co-transfecting with Lck were 9.8-, 15.0- or 5.6-fold higher, respectively, compared with WT WASP (Fig. 1C). On the other hand, these mutants by co-transfecting with another tyrosine kinase, Fyn, showed 3.3-, 4.4- or 2.1-fold higher phosphorylation of L270P, S272P or I294T WASP, respectively, compared with WT WASP (Fig. 1D). Together, these results showed that activating WASP mutants were susceptible to enhanced tyrosine phosphorylation by Src family tyrosine kinases and possessed higher actin polymerization activities *in vivo* compared with WT or Y291F WASP.

Activating WASP mutants demonstrate higher nuclear localization than WT or Y291F WASP

A putative nuclear localization signal (NLS) motif (KKRSGKKK) has been suggested in amino acid 225–232 of human WASP (25). Interspecies comparison of WASP showed that NLS motif, basic and GBD regions (amino acid 210–310) were highly conserved (Fig. 2A). Similar matching with reported NLS of N-WASP, a homolog of WASP, showed a slightly similar NLS, EKKKGKAKKKR to WASP (Fig. 2B). However, WASP is maintained in autoinhibited conformation through binding between GBD and VCA domain in resting state. Thus, we speculated that activating mutations in the GBD might disrupt the closed conformation and expose the NLS. To determine whether activating WASP mutants have different localization pattern from WT or Y291F WASP, COS-7 cells were transfected with EGFP-tagged WT, L270P, S272P, I294T or Y291F WASP. We failed to express the mutant that deleted whole NLS in COS-7 cells probably due to unstable protein. We could not identify critical basic residues because six basic residues, five lysine and one arginine, were in NLS of WASP. EGFP fluorescent intensities in the cytoplasm or nucleus were quantified by image processing software and the ratios were calculated as described in Methods. WT and Y291F WASP were mostly localized in the cytoplasm. In contrast, all three activating WASP mutants showed significantly lower cytoplasmic/nuclear ratio ($P < 0.01$) than WT and Y291F WASP, with some cells showing both cytoplasmic and nuclear localization (Fig. 2C and D).

WASP is co-immunoprecipitated with p54nrb and RNAP II

Since WASP could localize in the nucleus, we examined whether WASP interacted with any molecules in the nucleus. N-WASP has been shown to associate with p54nrb, an important nuclear molecule, which regulates RNAP II-dependent gene transcription in the nucleus (24). To examine whether p54nrb is a binding partner for WASP, we co-transfected Dsred-tagged p54nrb with EGFP-tagged WT WASP, L270P WASP or EGFP alone into COS-7 cells. Cell lysates were subjected to immunoprecipitation with anti-GFP or control IgG antibody. Figure 3(A) showed that both EGFP-tagged WT and L270P WASP were co-immunoprecipitated with p54nrb and RNAP II, but not in EGFP-transfected cells or immunoprecipitation with control IgG.

To examine whether WASP could localize with p54nrb in the nucleus, EGFP-WASP-transfected cells were fixed and subjected to immunofluorescence. Consistent with the results in Fig. 2(C and D), EGFP-WASP was localized in both cytoplasm and nucleus, and L270P WASP localized relatively more than WT WASP in the nucleus, in which exogenous p54nrb was exclusively expressed. Similar results were obtained in COS-7 cells transfected with HA-tagged WT and L270P WASP (Fig. 3B).

WASP binds to promoter region of genomic DNA

WASP could form a complex with p54nrb and RNAP II, indicating a role in gene transcription. Next, we examined whether WASP could bind to promoter region of genomic DNA. As WASP expression is restricted in hematopoietic cells and L270P WASP mutation in humans results in XLN (4, 5), we used a human myeloid cell line, K562, in which WASP expression is undetectable (Fig. 4A and B). We established several clones of K562 cells stably expressing WT or L270P WASP. Clones with comparable WASP expression levels were selected after verification by RT–PCR with WASP primers (Fig. 4A) and western blotting with anti-WASP antibody (Fig. 4B).

To examine subcellular localization of GFP-tagged WT or L270P WASP in K562 cells, equal numbers of cells were subjected to nuclear and cytoplasmic fractionation. As shown in Fig. 4(C), both of EGFP-tagged WT and L270P WASP, as well as actin, were detected in the nuclear fraction. Relatively higher ratio and 2.7-fold increase of nuclear WASP were observed in L270P WASP compared with WT WASP. Similar results were obtained in cells transfected with HA-tagged WT and L270P WASP, and 1.8-fold increase of nuclear WASP was observed in L270P WASP compared with WT WASP (Fig. 4D). Same samples were probed with vinculin and p54nrb or RNAP II to show that fractions were not a result of contamination of nuclear and cytoplasmic proteins, respectively.

Previous study showed N-WASP formed a complex with RNAP II and bound to GAPDH promoter (24). To examine whether WASP could bind to DNA in nucleus, lysates from WT or L270P WASP-expressing K562 cells were subjected to ChIP assay. DNA–protein complex was immunoprecipitated with anti-WASP, anti-RNAP II or control IgG antibodies. The immunoprecipitated DNA was analyzed by PCR using primers that amplify GAPDH promoter. Bands were highly detected in RNAP II immunoprecipitates compared with a relatively weak signal in WASP immunoprecipitates. No band was detected in control IgG immunoprecipitates or no template PCR negative control. Of note, PCR signal was relatively higher in L270P WASP compared with WT WASP, which could

be caused by increased WASP localization in the nucleus (Fig. 4E).

Distinct gene expression profile in WT or L270P WASP-transfected K562 cells

We next performed microarray analysis to investigate the gene expression profiles in K562 cells stably transfected WT and L270P WASP. Gene expression profiles of L270P-transfected K562 clones (MUT-1, MUT-2) were compared with the control WT WASP-transfected K562 clones (WT-1, WT-2) or the parental K562 as described in Methods. Pair numbers 6 and 10 were controls and genes overlapped in these groups were eliminated (Fig. 5A). Overall gene expression analysis through dot plot showed that WT-1 clone was closely

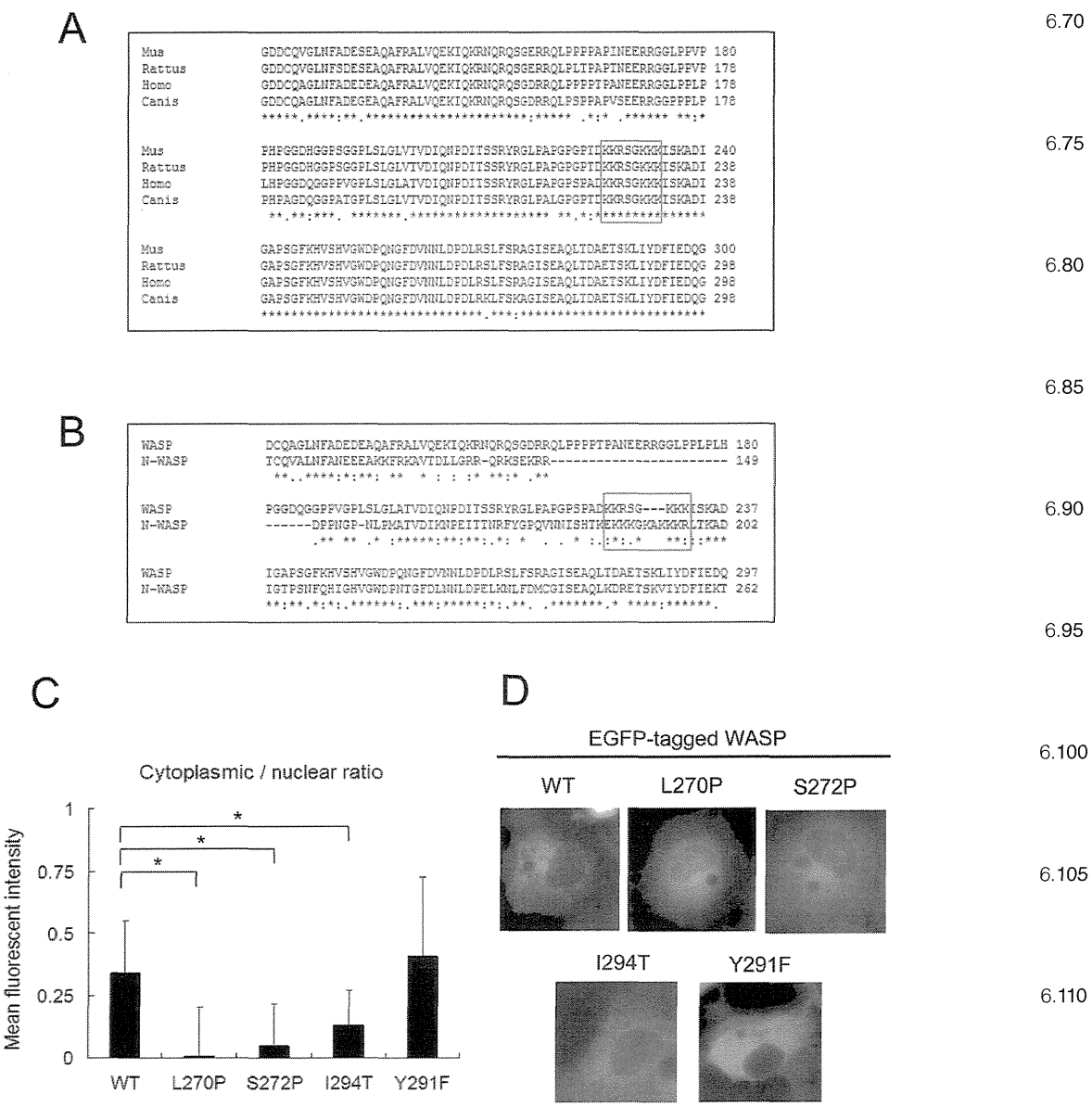

Fig. 2. Activating WASP mutants show higher nuclear localization ratio compared with WT or Y291F WASP. (A) Comparison of amino acid sequence in basic region and GBD of WASP among various species and (B) comparison of human WASP and N-WASP showed similar NLS. Red square boxes highlighted putative NLS. (C) COS-7 cells transfected with EGFP-tagged WT, L270P, S272P, I294T and Y291F WASP were subjected to fluorescent microscopy analysis. The cytoplasmic/nuclear ratio for each WASP construct was determined as described in Methods. Fifty cells were examined in each transfection and means ± SDs were shown in two independent experiments. Asterisks indicated statistically significant. (D) Representative GFP images showing subcellular localization of EGFP-tagged WT and mutants of WASP in COS-7 cells.

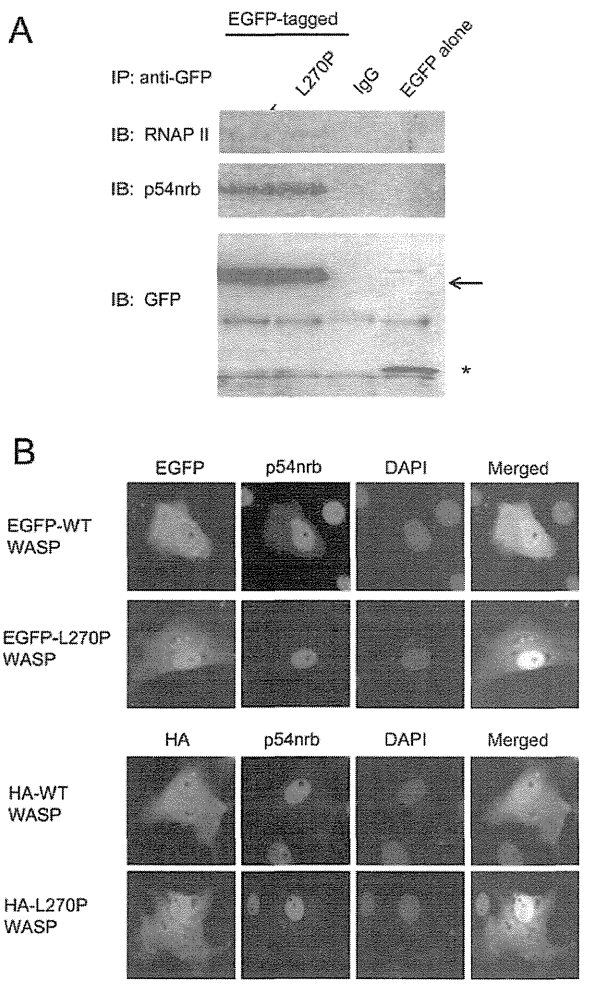

Fig. 3. WASP forms a complex with p54nrb and RNAP II. (A) EGFP-tagged WT, L270P WASP or EGFP alone and Dsred-tagged p54nrb were co-transfected into COS-7 cells. Immunoprecipitates with anti-GFP or control IgG (IgG) were probed with anti-RNAP II, anti-p54nrb and anti-GFP. Arrow indicated the bands of EGFP-tagged WT or L270P WASP and asterisk indicated the band of EGFP alone. (B) EGFP- or HA-tagged WT, L270P WASP and Dsred-tagged p54nrb transfected cells were subjected to immunofluorescence. Merged pictures of EGFP- or HA-tagged WASP (green) and p54nrb (red) were shown in right panels.

related to WT-2 clone, but remained distinct from MUT-1 and MUT-2 clones or the parental K562 (Fig. 5B). Next, scatter plots were used to identify genes that expression levels were significantly affected in each pair group (Fig. 5C). Total number of genes up-regulated or down-regulated >3-fold were 42 and 69 genes, respectively, in WT compared with L270P (MUT) WASP-transfected K562 clones. Based on gene annotations and functions including surface molecules, receptors, transcription factors, cytokines, integrins, cell cycle and signaling transduction, we showed that a number of genes in WT-1, WT-2 or MUT-1, MUT-2 clones were differentially regulated compared with the parental K562 cells (Fig. 5D).

To confirm the result of microarray analysis, we selected a few genes of interest and examined their expression levels by RT–PCR, western blotting or flowcytometry analysis using same clones used for microarray analysis. Interestingly, L270P WASP-transfected K562 cells showed a higher mRNA expression of protein tyrosine phosphatase receptor c (PTPRC/CD45) compared with the parental or WT WASP-transfected K562 cells (Fig. 6A). In addition, representative flowcytometry analysis demonstrated higher protein expression level of CD45 in L270P WASP-transfected clone (Fig. 6D). On the other hand, mRNA and protein level of Runx1 (Fig. 6A and B) or G-CSFR (Fig. 6A and C) were increased in WT WASP-transfected K562 cells, but not in parental or L270P WASP-transfected K562 cells.

Different binding affinity to genomic DNA binding region of WT or L270P WASP

To examine whether WT or L270P WASP bound to the promoter region of the genes examined in Fig. 6, we performed ChIP on chip analysis using WT or L270P WASP-transfected K562 cells. DNA–protein complex was immunoprecipitated with highly specific anti-WASP 5A5 mAb and the immunoprecipitated DNA was hybridized to DNA chips. Scatter plots of ChIP on chip data revealed that WT or L270P WASP bound to vast array of genes covering chromosomes 1–22, X and Y (Fig. 7A). DNA binding regions of PTPRC (CD45), G-CSFR and Runx1 by WT WASP or L270P WASP were vastly differing among these genes, ranging from promoter regions to introns and exons. By analyzing these genes, we found a highly similar DNA binding pattern between WT and L270P WASP, but different binding affinity at the same locus. L270P WASP bound to PTPRC (CD45) significantly stronger and it bound to G-CSFR and Runx1 weaker than WT WASP (Fig. 7B–D), while it showed similar binding affinity to the housekeeping gene, GAPDH (Fig. 7E). These results were consistent with our data that L270P WASP up-regulated PTPRC (CD45) expression while WT WASP up-regulated G-CSFR and Runx1 expression, suggesting that WT or L270P WASP promoted different gene expression by altered DNA binding affinity at the same locus.

Discussion

In this study, we showed that WASP was present both in the cytoplasm and the nucleus, similar to other WASP family members, N-WASP and WAVE1 (21, 24, 26, 27), and regulated gene transcription in myeloid cells.

The nucleus and cytoplasm are separated by the nuclear membrane containing nuclear pore complex. Molecules <40kDa can diffuse passively through the nuclear pore while larger molecules require facilitated transport mechanisms (28). WASP is a 60-kDa protein that contains a cluster of positively charged basic amino acids (KKRSGKKK) corresponding to amino acid 225–232 as putative NLS. We showed that the NLS of WASP was highly conserved among species. Comparison between WASP and its family member proteins showed that NLS of WASP was resemble to N-WASP, but totally different from WAVE1, indicating other nuclear transport mechanisms could be utilized by WAVE1.

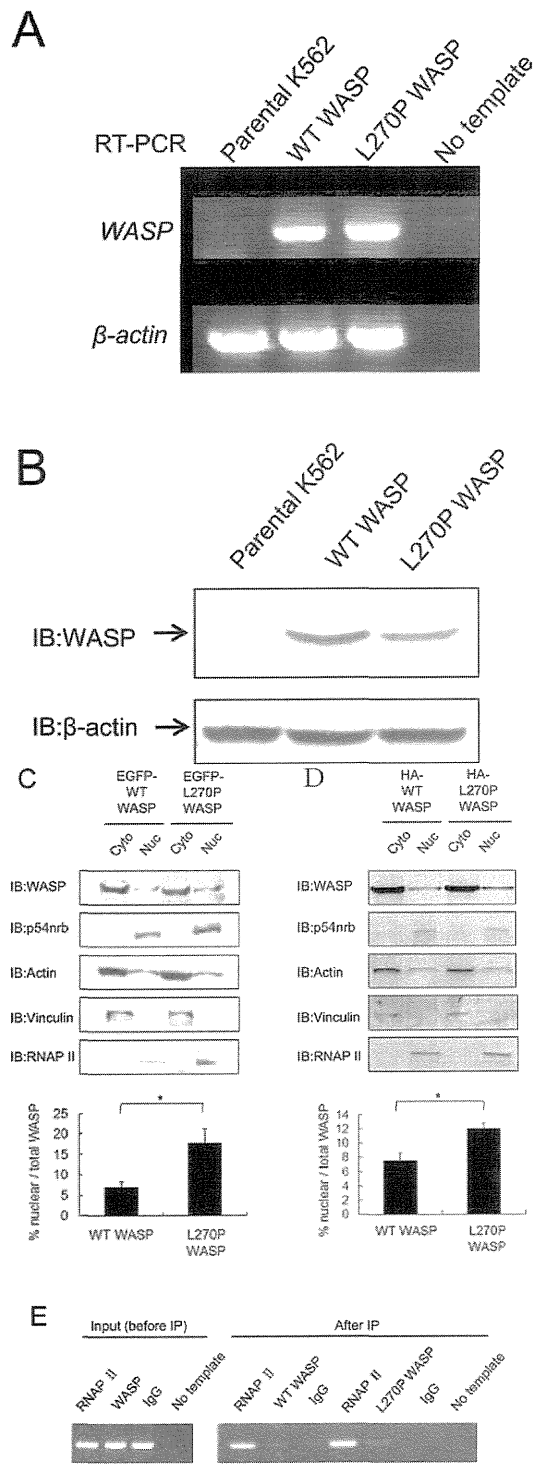

Fig. 4. WASP binds to promoter DNA in K562 cells. (A and B) Expression of WT or L270P WASP in parental K562 cells and stably transfected clones were confirmed by (A) RT–PCR analysis with WASP or β-actin primers and (B) western blotting analysis with anti-WASP or anti-β-actin antibodies. Expected bands were indicated by arrows. (C and D) K562 clones stably transfected with EGFP-tagged WT or L270P WASP (C) and HA-tagged WT or L270P WASP (D) were subjected to cytoplasmic (Cyto) and nuclear (Nuc) fractionation and probed with anti-WASP, p54nrb, actin, vinculin and RNAP II antibodies. Lower panels showed the percentages of nuclear WASP relative to total amount of WASP. Means ± SDs were shown in two independent experiments. Asterisk indicated statistical significance. (E) ChIP assays were performed with anti-RNAP II (RNAP II), anti-WASP (WASP) or control IgG (IgG) antibodies. Input (left) or immunoprecipitated DNA (right) was subjected to PCR analysis using primers for GAPDH promoter. Sterile water (no template) was used as negative control.

Similar matching with reported NLS of N-WASP, a homolog of WASP, showed a slightly different amino acid composition, EKKKGKAKKKR, in the basic region.

We presented here that three constitutively activating WASP mutants had enhanced tyrosine phosphorylation, higher actin polymerization activities, and showed lower cytoplasmic/nuclear ratio compared with WT or Y291F WASP. NLS and Y291 of WASP could be masked in the autoinhibitory conformation of WASP through hydrophobic interaction between VCA domain and the GBD in inactivated cells (17). Activating signals or constitutively activating mutations have been shown to disrupt the closed conformation between GBD and VCA domain (5), which may in turn expose the NLS that allows more nuclear translocation of WASP through nuclear pores. Open conformation may also expose Y291 to Src family tyrosine kinases, resulting in enhanced tyrosine phosphorylation and Arp2/3-mediated actin polymerization (29, 30). Thus, the autoinhibited conformation is important for safeguarding WASP from unwanted activation and for accurate regulation of subcellular localization in order to exert its function in the proper cellular compartment.

At present, studies on functions of WASP in the nucleus remain to be investigated. We showed that WASP was co-immunoprecipitated with p54nrb and RNAP II, similar to its homolog N-WASP (24). N-WASP is ubiquitously expressed, whereas WASP expression is restricted in hematopoietic cells (3). Thus, loss of function due to WASP mutation primarily affects hematopoietic cells. It is demonstrated by a recent study that knockout of WASP leads to down-regulate gene transcription of master genes for T_h1 cell differentiation in the nucleus (25). It is noteworthy that N-WASP knockout mice are embryonic lethal suggesting its broad biological importance especially in development and not restricted to hematopoietic cell function and differentiation (31).

Although we showed that both WT and L270P WASP could bind to DNA, we speculated that DNA binding could be indirect through p54nrb or RNAP II. WASP has no known putative DNA binding motifs, whereas p54nrb contains two RNA recognition motif domains that can bind to nucleic acids and proteins (32). The interaction between WASP and p54nrb may not play a major role in the effects of WASP in open configuration on gene transcription because binding affinity of L270P WASP to p54nrb is similar to that of WT WASP. p54nrb, together with PSF (polypyrimidine tract-binding protein-associated splicing factor), can bind to the C-terminal domain of the largest subunit of RNAP II and mediate contacts between RNAP II and small nuclear ribonucleoproteins (snRNPs)

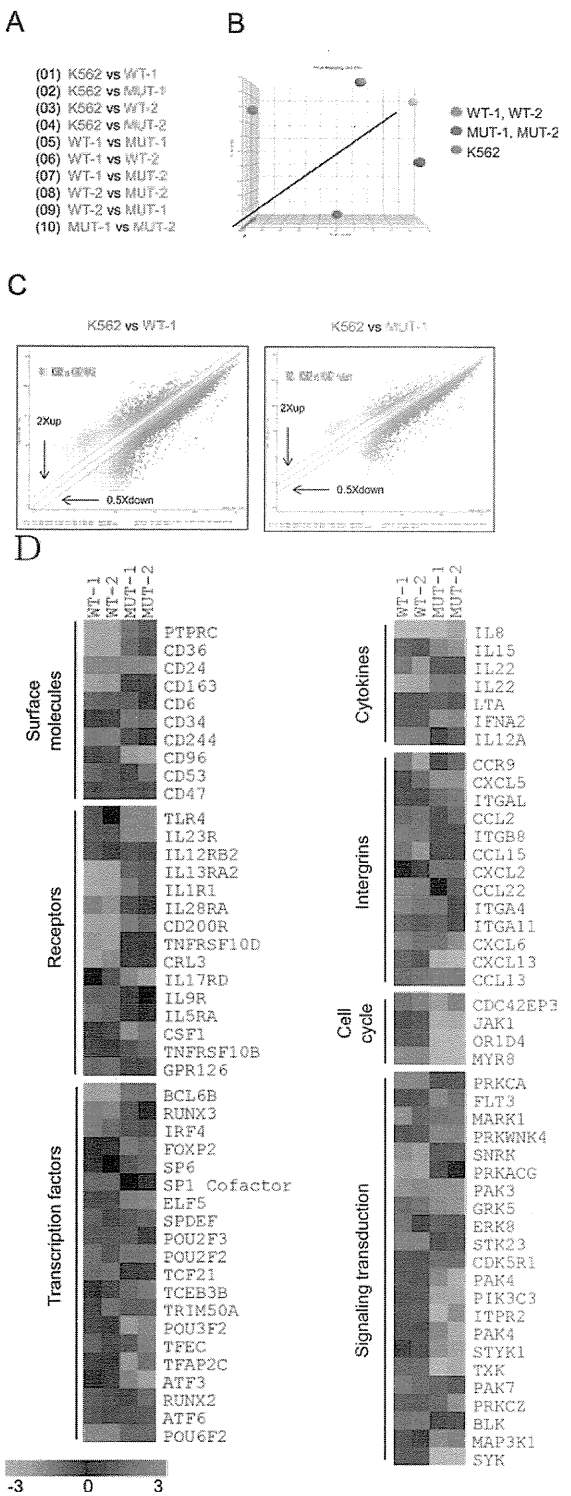

Fig. 5. Microarray analysis of K562 clones stably transfected with WT or L270P WASP compared with parental K562 cells. (A) Groups in pairs showing parental K562 compared with two clones expressing either WT WASP (WT-1, WT-2) or L270P WASP (MUT-1, MUT-2). Pairs 6 and 10 are internal control groups. (B) Comparison of overall expression profiles of WT WASP (red dots) and L270P WASP (blue dots) with parental K562 (green) as standard. (C) Scatter plots showing gene expression in pair 1: K562 versus WT-1 (left) and pair 2: K562 versus MUT-1 (right) (upper line showing 2× up-regulation and lower line showing 0.5× down-regulation). (D) Selected genes differentially expressed in WT or L270P WASP-transfected K562 cells were grouped according to their functions in cells.

during the coupled transcription and splicing process (33). As gene transcription involves a myriad of transcription factors and molecules binding to the promoter, WASP may provide a scaffold recruiting different transcription factors required for efficient and proper gene transcription. Indeed, Taylor et al. reported that WASP associated with the histone-modifying proteins, H3K4 trimethyltransferase and H3K9/H3K36 tridemethylase, which are recruited and achieved transcription-permissive chromatin dynamics at the T-bet master gene T-box transcription factor 21 (TBX21) promoter region. Therefore, knockout of WASP led to down-regulate gene transcription of master genes important for T-bet cell differentiation in the nucleus (25). We examined whether genes critical for T-bet cell differentiation were included in the list of altered gene expression between WT and L270P WASP-transfected K562 cells. However, we could not identify significant genes involved in T-bet cell differentiation, probably due to different pairs of comparison in different cell lineages.

Gene transcription is regulated by a complex network of genes. Our results showed that L270P WASP-transfected K562 cells demonstrated a distinct gene expression profile compared with WT WASP-transfected or parental K562 cells. We showed that both WT and L270P WASP were co-immunoprecipitated with p54nrb and RNAP II. Nuclear WASP could activate certain molecules or mechanisms that contribute to differential expression profiles. For example, nuclear N-WASP has been shown to modulate the expression of heat shock protein 90, which in turn regulates Src tyrosine kinase Fyn (26). Through microarray and western blot analysis, we found that PTPRC (CD45), a molecule that regulated activity of Src family tyrosine kinases such as Lck or Fyn, was differentially expressed in WT and L270P WASP-transfected K562 cells. In fact, K562 cells expressing L270P WASP had higher CD45 expression, implying a possible negative feedback loop to attenuate tyrosine kinase activities in these cells to counter the effect of constitutively activating mutation of WASP.

In some cases, patients with loss-of-function WASP mutations developed malignant lymphoma and other malignant diseases (34–36), whereas the rare gain-of-function activating WASP mutations have been linked to XLN and myelodysplastic syndrome (4, 5). These observations could not be sufficiently explained by the function of WASP as actin regulator in the cytoplasm. We have shown that WASP was co-immunoprecipitated with DNA. Moulding et al. (37) showed that WASP could play a role in cell division where uncontrolled actin polymerization by activating mutating WASP I294T caused defects in mitosis and cytokinesis, and led to decreased proliferation and increased apoptosis. These suggest that WASP dysfunction results in dysregulated cellular

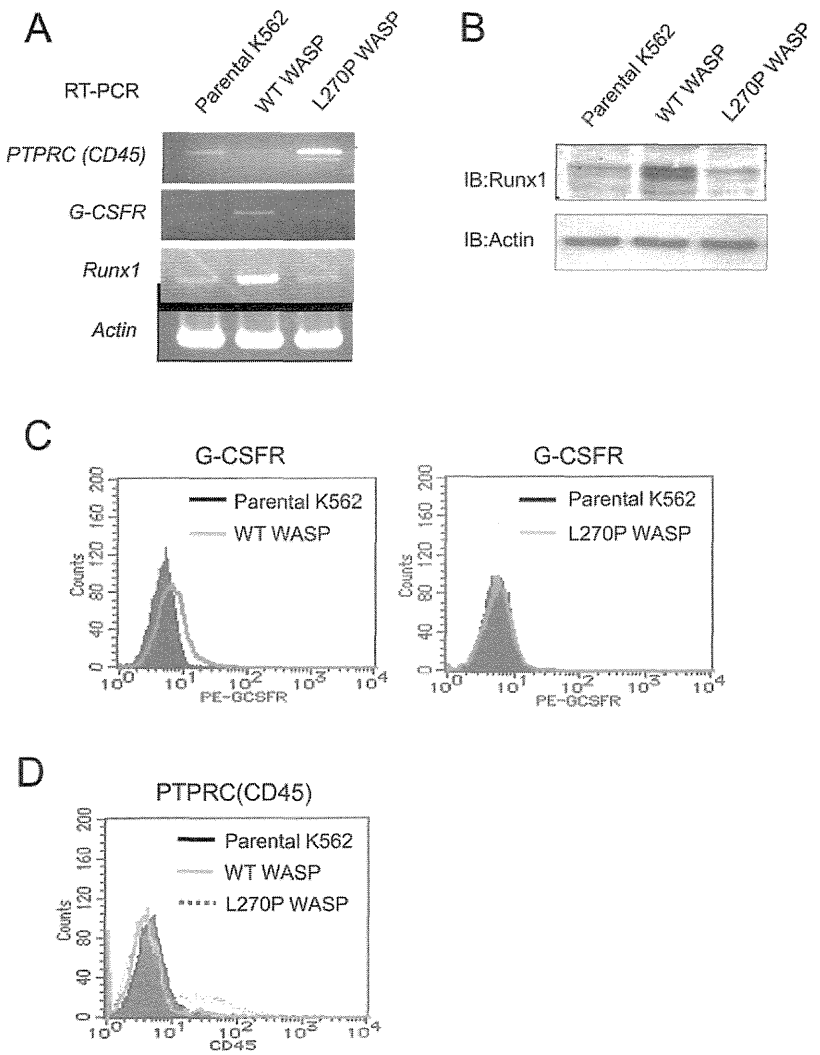

Fig. 6. *Determination of mRNA and protein levels of selected genes in WASP expressing K562 cells.* (A) RT–PCR analysis of mRNA levels of PTPRC (CD45), G-CSFR and Runx1 compared with β-actin control in parental, WT or L270P WASP-transfected K562 clones. (B) Western blot analysis of protein levels of Runx1 compared with β-actin. (C and D) Flowcytometry analysis of protein expression levels of (C) G-CSFR and (D) PTPRC (CD45).

cytokinesis and genomic instability. However, it is unknown why only myeloid cells are highly susceptible to apoptosis as WASP is also expressed in lymphoid lineage. Of note, we noticed some clones with over-expression of L270P WASP did not lead to cell death or growth inhibition. Moreover, microarray analysis data showed that apoptosis-related genes such as caspase-9 and Bcl-2 were not significantly affected. Flowcytometry analysis by annexin V staining did not reveal significant different apoptotic rate between WT and L270P WASP-transfected K562 cells (data not shown). Through ChIP on chip assay, we showed that WT or L270P WASP had distinct binding affinity to DNA. Thus, we speculated that L270P WASP could affect normal gene transcription, which is important for myeloid cell differentiation and proliferation. For example, Runx1 and G-CSFR, genes important for definitive hematopoiesis and terminal differentiation of promyelocytes to granulocytes, respectively, were up-regulated in WT WASP-transfected K562 cells but not in L270P WASP-transfected K562 cells.

Our study provided evidence that open conformation of WASP could result in enhanced tyrosine phosphorylation, higher actin polymerization activities and more localization in the nucleus compared with WT WASP. We showed that WASP regulated gene transcription in myeloid cells. Previous study reported the function of N-WASP and its nuclear binding molecules in promoting actin polymerization in the nucleus and RNAP II-dependent transcriptional regulation (24). Thus, it is interesting to explore the function of activating WASP mutants

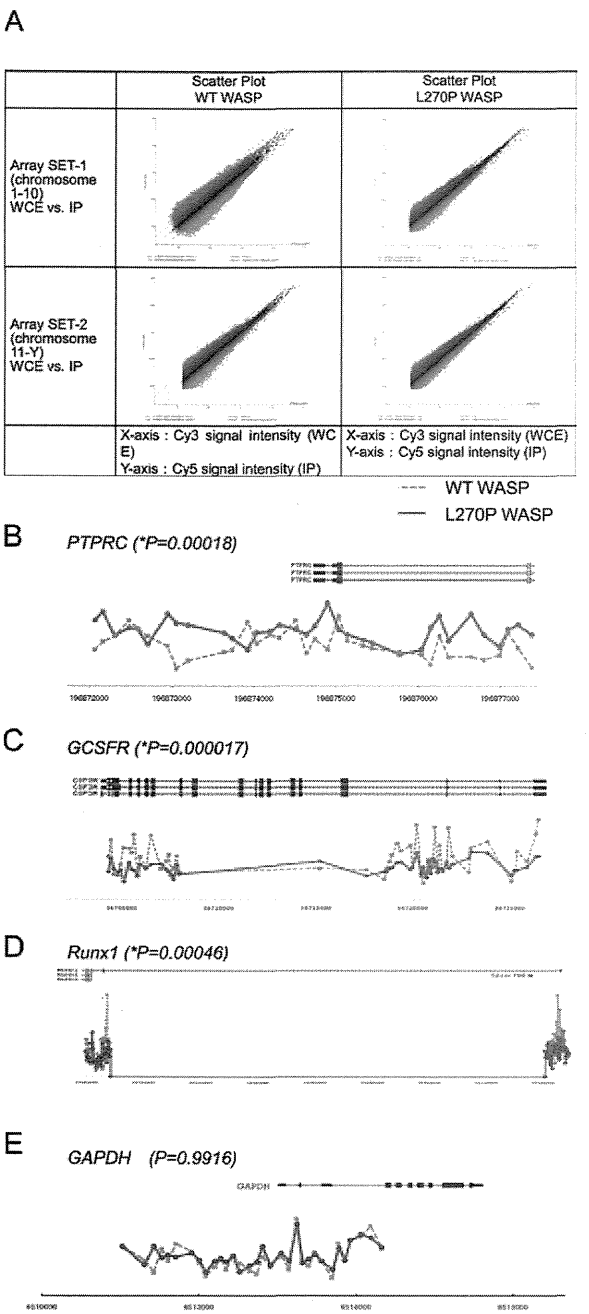

Fig. 7. ChIP on chip analysis of DNA binding region of L270P WASP compared with WT WASP. (A) Scatter plots of ChIP on chip data of whole cell extracts (WCE) and immunoprecipitates (IP) in WT and L270P WASP-transfected K562 clones in chromosomes 1–10 (upper) and 11-Y (lower). (B–D) Comparison of binding affinity with genomic DNA binding regions between WT WASP (gray) and L270P WASP (red) in (B) PTPRC (CD45), (C) G-CSFR, (D) Runx1 and (E) control housekeeping gene GAPDH. Genomic structures of each gene were shown in blue. Differences of the binding affinity between WT and L270P WASP were examined by *P* value and asterisks indicated statistically significant.

in the nucleus in future research to assist in the understanding how aberrant function of nuclear WASP is translated into clinical defects.

Funding

Ministry of Education, Culture, Sports, Science and Technology of Japan (20591242, 23591528 to Y.S.); Ministry of Health, Labour and Welfare of Japan (003 to Y.S. and S.T.); Mother and Child Health Foundation (21-6 to Y.S.); Japan Foundation for Pediatric Research (10-007 to Y.S.).

Acknowledgements

We would like to thank Drs K. A. Siminovitch, M. Satake and N. Ishii for reagents, Drs A. J. Thrasher and T. Takai for their helpful comments.

References

1 Aldrich, R. A., Steinberg, A. G. and Campbell, D. C. 1954. Pedigree demonstrating a sex-linked recessive condition characterized by draining ears, eczematoid dermatitis and bloody diarrhea. *Pediatrics* 13:133.
2 Derry, J. M., Ochs, H. D. and Francke, U. 1994. Isolation of a novel gene mutated in Wiskott-Aldrich syndrome. *Cell* 78:635.
3 Stewart, D. M., Treiber-Held, S., Kurman, C. C., Facchetti, F., Notarangelo, L. D. and Nelson, D. L. 1996. Studies of the expression of the Wiskott-Aldrich syndrome protein. *J. Clin. Invest.* 97:2627.
4 Ancliff, P. J., Blundell, M. P., Cory, G. O. *et al.* 2006. Two novel activating mutations in the Wiskott-Aldrich syndrome protein result in congenital neutropenia. *Blood* 108:2182.
5 Devriendt, K., Kim, A. S., Mathijs, G. *et al.* 2001. Constitutively activating mutation in WASP causes X-linked severe congenital neutropenia. *Nat. Genet.* 27:313.
6 Thrasher, A. J. and Burns, S. O. 2010. WASP: a key immunological multitasker. *Nat. Rev. Immunol.* 10:182.
7 Hüfner, K., Higgs, H. N., Pollard, T. D., Jacobi, C., Aepfelbacher, M. and Linder, S. 2001. The verprolin-like central (vc) region of Wiskott-Aldrich syndrome protein induces Arp2/3 complex-dependent actin nucleation. *J. Biol. Chem.* 276:35761.
8 Higgs, H. N., Blanchoin, L. and Pollard, T. D. 1999. Influence of the C terminus of Wiskott-Aldrich syndrome protein (WASp) and the Arp2/3 complex on actin polymerization. *Biochemistry* 38:15212.
9 Burns, S., Cory, G. O., Vainchenker, W. and Thrasher, A. J. 2004. Mechanisms of WASp-mediated hematologic and immunologic disease. *Blood* 104:3454.
10 Bouma, G., Burns, S. and Thrasher, A. J. 2007. Impaired T-cell priming *in vivo* resulting from dysfunction of WASp-deficient dendritic cells. *Blood* 110:4278.
11 Gallego, M. D., de la Fuente, M. A., Anton, I. M., Snapper, S., Fuhlbrigge, R. and Geha, R. S. 2006. WIP and WASP play complementary roles in T cell homing and chemotaxis to SDF-1alpha. *Int. Immunol.* 18:221.
12 Gallego, M. D., Santamaría, M., Peña, J. and Molina, I. J. 1997. Defective actin reorganization and polymerization of Wiskott-Aldrich T cells in response to CD3-mediated stimulation. *Blood* 90:3089.
13 Snapper, S. B., Rosen, F. S., Mizoguchi, E. *et al.* 1998. Wiskott-Aldrich syndrome protein-deficient mice reveal a role for WASP in T but not B cell activation. *Immunity* 9:81.
14 Zhang, J., Shehabeldin, A., da Cruz, L. A. *et al.* 1999. Antigen receptor-induced activation and cytoskeletal rearrangement are impaired in Wiskott-Aldrich syndrome protein-deficient lymphocytes. *J. Exp. Med.* 190:1329.
15 Lorenzi, R., Brickell, P. M., Katz, D. R., Kinnon, C. and Thrasher, A. J. 2000. Wiskott-Aldrich syndrome protein is necessary for efficient IgG-mediated phagocytosis. *Blood* 95:2943.
16 Westerberg, L. S., Meelu, P., Baptista, M. *et al.* 2010. Activating WASP mutations associated with X-linked neutropenia result in